High-throughput synthesis and specificity characterization of natively paired antibodies using oPool+ display

Wenhao O. Ouyang[1], Huibin Lv[1,2], Wenkan Liu[1], Ruipeng Lei[1], Zongjun Mou[3], Tossapol Pholcharee[1], Logan Talmage[1], Meixuan Tong[1], Yiquan Wang[1], Katrine E. Dailey[1], Akshita B. Gopal[1], Danbi Choi[1], Madison R. Ardagh[1], Lucia A. Rodriguez[1], Xinghong Dai[3], Nicholas C. Wu[1,2,4,5,*]

Affiliations:

[1] Department of Biochemistry, University of Illinois at Urbana-Champaign, Urbana, IL 61801, USA

[2] Carl R. Woese Institute for Genomic Biology, University of Illinois at Urbana-Champaign, Urbana, IL 61801, USA

[3] Department of Physiology and Biophysics, Case Western Reserve University, School of Medicine, Cleveland, OH 44106, USA

[4] Center for Biophysics and Quantitative Biology, University of Illinois at Urbana-Champaign, Urbana, IL 61801, USA

[5] Carle Illinois College of Medicine, University of Illinois at Urbana-Champaign, Urbana, IL 61801, USA

*To whom correspondence should be addressed. Email: nicwu@illinois.edu (N.C.W.)

ABSTRACT

Antibody discovery is crucial for developing therapeutics and vaccines as well as understanding adaptive immunity. However, the lack of approaches to synthesize antibodies with defined sequences in a high-throughput manner represents a major bottleneck in antibody discovery. Here, we presented oPool^{+} display, a high-throughput cell-free platform that combined oligo pool synthesis and mRNA display to rapidly construct and characterize many natively paired antibodies in parallel. As a proof-of-concept, we applied oPool^{+} display to probe the binding specificity of >300 uncommon influenza hemagglutinin (HA) antibodies against 9 HA variants through 16 different screens. Over 5,000 binding tests were performed in 3-5 days with further scaling potential. Follow-up structural analysis of two HA stem antibodies revealed the previously unknown versatility of IGHD3-3 gene segment in recognizing the HA stem. Overall, this study established an experimental platform that not only accelerate antibody characterization, but also enable unbiased discovery of antibody molecular signatures.

Keywords: High-throughput screening, influenza, hemagglutinin, B-cell receptors, antibody, broadly neutralizing, oligo pools, mRNA display, cryo-EM

INTRODUCTION

Antibodies are central to the immune system for protection against pathogen infection. Therefore, identification of antibodies that target pathogens of interest is key to the understanding of adaptive immunity as well as the development of effective therapeutics and vaccines. In recent years, advances in single-cell B-cell receptor sequencing (scBCR-seq) have greatly improved the capacity to discover novel antibodies[1]. Thousands of natively paired antibody sequences can be obtained from a single scBCR-seq experiment. By contrast, downstream characterization of these antibody sequences remains costly, labor intensive, and time consuming, involving cloning, expression, purification, and testing the binding activities of different antibodies individually. At the same time, protein display technologies offer a high-throughput solution for characterizing antibody binding activity[2], with antibody library construction being an essential first step. Methods for constructing antibody libraries with random heavy-light chain pairing from B cell repertoires are well-established[3,4]. However, there is a lack of approaches to synthesize custom-made antibody libraries with precise heavy-light chain pairing from a defined list of antibody sequences. This technical barrier has restricted the application of protein display technologies in antibody research, including large-scale characterization of previously discovered antibodies.

Hemagglutinin (HA) is the major antigen of influenza A and B viruses. Influenza A HA is further divided into two groups with a total of 19 antigenic subtypes (H1-H19). Group 1 HA includes H1, H2, H5, H6, H8, H9, H11, H12, H13, H16, H17, H18, and H19, whereas group 2 HA includes H3, H4, H7, H10, H14, and H15. HA is a homotrimeric glycoprotein consisting of a hypervariable globular head domain atop a conserved stem domain[5,6]. The functions of HA are critical for viral entry. The globular head domain engages the sialylated receptor, whereas the stem domain possesses the membrane fusion machinery. In the past two decades, many human antibodies to the HA stem have been discovered and characterized[7–11]. In contrast to HA head antibodies, which are usually strain-specific, HA stem antibodies often cross-neutralize multiple influenza subtypes. Several recurring sequence features have

been observed among HA antibodies isolated from different individuals, such as IGHV1-69, IGHV1-18, IGHD6-1, IGHD3-9 for stem antibodies, and IGHV2-70 and IGHD4-17 for head antibodies[7,11–15]. However, many HA antibodies do not contain any known recurring sequence features, suggesting there are additional features yet to be discovered. Discovering the recurring sequence features of HA antibodies is critical for the molecular understanding of antibody responses at the population level, which will in turn benefit the development of universal influenza vaccines.

In this study, we developed oPool^{+} display, a rapid and cost-effective cell-free platform that combined oligo pool synthesis with mRNA display to assemble and screen natively paired antibodies in a highly parallel manner. As a proof-of-concept, we first synthesized a library of 325 natively paired HA antibodies with uncommon germline gene usages, then characterized their binding activity to seven different HAs from influenza A and B viruses as well as an H1 stem construct and an H3 stem construct. We also carried out competition screens against a known HA stem antibody for binding to the same set of HAs, allowing epitope inference. Our screening showed that 114 of the 325 antibodies bound to at least one of the nine HA screened, 45 of which were further identified as HA stem antibody candidates. Extensive experimental validations confirmed the robust performance oPool^{+} display. We then demonstrated oPool^{+} display's potential in discovering antibody sequence features through structural and functional characterizations of 16.ND.92 and AG11-2F01, two group 1 stem antibody enriched in the screen. 16.ND.92 and AG11-2F01 exhibited distinct binding modes of IGHD3-3 to HA stem, yet both antibodies were broadly reactive and protected against lethal influenza challenge *in vivo*. This observation substantiated that IGHD3-3 is a recurring sequence feature of HA stem antibodies and demonstrated its versatility in binding to HA stem.

RESULTS

High throughput assembly of natively paired antibody library via oligo pools

We previously curated a dataset containing 5,561 human monoclonal HA antibodies, 1,082 (19.5%) of which are known to bind to either the head domain or the stem domain[16]. Of the remaining 4,479 (80.5%) HA antibodies which lack epitope information, 292 have complete heavy chain variable (V_H) and light chain variable (V_L) sequences available and are not encoded by well-characterized sequence features of HA stem antibodies, namely IGHV1-69, IGHV1-18, IGHV6-1, and IGHD3-9[7,12–14] (**Figure S1A and Table S1**). These 292 HA antibodies were included in the synthesis of our natively paired antibody library. In addition, three known stem antibodies, namely 31.a.55, AG11-2F01, and 042-100809-2F04[7,17], as well as 30 known HA head antibodies[6,15,18–25] were included as controls, bringing the total library size to 325 antibodies **(Figure 1A)**.

To synthesize the natively paired antibody library in a high-throughput manner, we aimed to leverage recent advances in oligo pool synthesis. The maximum length of each oligo in commercial oligo pool synthesis is around 300 to 350 nucleotides. By contrast, the length of a single-chain variable fragment (scFv), which is the smallest format of a human antibody, is around 800 to 900 nucleotides. As a result, each given scFv sequence was split into 4 oligos with overlaps at the diverse complementary-determining regions (CDRs), namely the CDRs H1, H3, and L3 (**Figure 1B-C and Table S2**). We then performed codon randomization to ensure that the overlaps among oligos for the same scFv are unique at the nucleic acid level. This would help prevent mis-annealing between oligos from different scFvs, especially if they shared similar amino acid sequences (**Figure 1B, Material and Methods**). Through an one-pot overlap PCR, full-length scFv sequences could then be generated with the intended native V_H and V_L pairing. Subsequently, this strategy was applied to design the oligo pools for our library of 325 antibodies (**Figure 1C-F, Figure S1B-C, and Table S2**).

The length of the assembled product was consistent with that of full-length scFvs (**Figure 1D**). To thoroughly evaluate the effectiveness of our synthesis strategy, we then performed several assembly PCRs with the starting oligos of 25, 75, 100, 125, 150, and 200 scFvs

each in a single tube (**Figure 1E-F and Figure S2**). PacBio sequencing revealed the high reproducibility of the one-pot PCR assembly across the board, with a Pearson correlation coefficient of 0.95 even at 200 scFvs per PCR (**Figure 1E**). The one-pot PCR assembly strategy also achieved high coverage of the targeted antibodies, with only a subtle drop from 100% to 90% as the complexity of the PCR increased from 25 to 200 scFvs (**Figure 1F**). For our final library of all 325 scFvs, a Pearson correlation coefficient of 0.83 was observed between replicates, with a coverage of 322 of 325 (99.1%) natively paired antibodies (**Figure S3**). While we opted to assemble this antibody library through 13 PCRs with 25 scFvs each tube, our results demonstrated the potential to further increase the throughput of our antibody library synthesis strategy by at least one orders of magnitude.

Rapid specificity characterization of the natively paired antibodies by mRNA display

To characterize antibody specificity from our natively paired scFv library, we utilized mRNA display[26–28], a well-established cell-free screening approach that allows rapid screening for protein binders. Briefly, each scFv was covalently linked to the RNA molecule that encoded it, thus providing a phenotype-genotype linkage (**Figure S4A, Material and Methods**). The mRNA-displayed antibody library was then selected against seven HAs from different influenza A subtypes and influenza B strains, namely H1N1 A/Solomon Island/3/06 (H1/SI06), H1N1 A/Michigan/45/2015 (H1/MI15), H3N2 A/Singapore/INFIMH-16-0019/2016 (H3/SP16), H5N1 A/ Qinghai/1A/2005 (H5/QH05), H7N9 A/Shanghai/2/2013 (H7/SH13), B/Phuket/3073/2013 (B/Phu13), and B/Lee/1940 (B/Lee40). Selections were also performed against two HA stem domain constructs that were designed based on H1N1 A/Brisbane/59/2007 HA and H3N2 A/Finland/486/2004 HA, respectively[29,30] (**Figure 2 and Figure S4**). After one round of selection, the pre- and post-selection libraries were then analyzed by PacBio sequencing to quantify the enrichment of each scFv (**Table S3**). Pearson correlation coefficients ranging from 0.58 to 0.86 were observed between biological replicates (**Figure S5**), demonstrating the reproducibility of the selections. In total, 114 of the 325 scFvs were identified to target one of the HAs screened, with 52 targeting more than

one HA and 11 targeting more than two HAs (**Table S4**). All stem antibody controls were enriched in at least one screens, while only 17 of the 30 head antibody controls were enriched, likely due to the considerably limited binding breadth of head antibodies. Moreover, the stem antibody controls were highly enriched in the selections against the HA stem domain constructs, whereas the head antibody controls were not, further validating that selection took place.

We also performed seven competition screens against CR9114[10], a broadly neutralizing HA stem antibody, for binding to H1/SI06, H1/MI15, H3/SP16, H5/QH05, H7/SH13, and B/Phu13, and B/Lee40 (**Figure 2 and Figure S6**). Competition screens were performed using the same protocol as the mRNA display selections described above, except that CR9114 was pre-bound to the HAs. While the CR9114 competition screen for H3/SP16 did not yield consistent PCR bands post-selection, all six other screens resulted in reproducible bands and were analyzed by PacBio sequencing. Of these six screens, five had Pearson correlation coefficients of >0.7 between replicates (**Figure S7**), demonstrating their reproducibility. The results of our competition screening were in agreement with previous studies. For example, two of our stem antibody controls, AG11-2F01 and 31.a.55, competed with CR9114 in our screens, which is consistent with previous studies of these two antibodies[7,17]. Additionally, 15 of the 17 (88%) HA head antibody controls targeting at least one HA in our screens did not compete with CR9114, further supporting the effectiveness of the competition screen (**Table S4**). Together, we identified five antibody candidate targeting group 1 HA stem, 12 targeting group 2 HA stem, as well as 28 targeting influenza B HA stem (**Figure S5 and Table S4**). Of note, one of the H3 stem antibody candidates, AG2-G02, was concurrently identified by a machine learning approach and experimentally confirmed in another study of ours[16].

oPool^{+} display demonstrates robust performance in specificity characterization

To systematically evaluate the performance of oPool$^+$ display, we used both biolayer interferometry (BLI) and ELISA to validate the binding activities of selected antibodies (**Figure 3**). In brief, 25 antibodies were selected, recombinantly expressed and purified in fragment antigen-binding (Fab) and IgG formats. Their binding activities were then tested against all nine HAs used in our screens (**Figure 3A-B, Figure S8**). This validation experiment substantiated the robust performance of oPool$^+$ display. A true positive rate of 80.4% (41/51) and a true negative rate of 95.4% (166/174) was observed in BLI validation with Fabs, while a true positive rate of 71.7% (43/60) and a true negative rate of 96.4% (159/165) was observed in ELISA validation with IgG (**Figure 3C**). Of note, both experimental validations indicated that the majority of the false positive and false negative results (11/18 for BLI, 14/23 for ELISA) were from three screens (H3 stem, H1/SI06, and H1/MI15). To examine the influences of different antibody formats on binding, we determined the dissociation constant (K_D) of three H1 stem antibodies and six H3 stem antibodies that were enriched in our screen in both Fab and scFv formats (**Figure 3D, Figure S9 and S10**). All nine antibodies retained binding in both formats, with no apparent correlation between the K_D values. However, some of the false negatives could still be due to weakened binding of the antibody in scFv format during the screens.

We then further assessed the performance of our CR9114 competition screens using 16 of the 25 antibodies validated above (**Figure 4A-B**). To quantify the competition, we first defined the CR9114 competition index as the log fold change of enrichments with versus without the presence of CR9114 during screen (**Table S4, Figure S11, Materials and Methods**). A higher CR9114 competition index would indicate overlapping epitopes between the scFv and CR9114, while a lower CR9114 competition index would indicate opposite (**Figure 4A**). Experimental validation of these competition indices was then performed using BLI, where the ratio of binding responses to HA with and without CR9114 pre-bound was quantified (**Materials and Methods**). Pearson correlation of 0.66 was observed between the competition indices and the validation results (**Figure 4B, Figure S12, and Table S5**),

206 confirming the reliability of our CR9114 competition screens. Together, our results showed
207 that oPool^{+} display enabled rapid and accurate specificity characterization of natively paired
208 antibodies.
209
210 **AG11-2F01 and 16.ND.92 have similar sequence features but distinct binding modes**
211 One of the H1 stem antibodies identified from our screen was 16.ND.92, which was
212 originally isolated from a young individual in an H5N1 influenza vaccine trial[7]. 16.ND.92 was
213 encoded by IGHV3-74/IGHD3-3/IGKV1-5 (**Table S4**). Coincidentally, both IGHD3-3 and
214 IGKV1-5 were utilized by AG11-2F01, which was one of the two positive controls against H1
215 stem in our screen (**Figure 2 and Figure S5**). Moreover, 16.ND.92 and AG11-2F01 shared a
216 similar FG[V/L] motif encoded by the reading frame +3 of IGHD3-3 (**Figure S13**). This
217 observation led us to hypothesize that 16.ND.92 and AG11-2F01 engaged the HA stem via
218 similar binding modes. Consequently, we determined the cryo-EM structures of H1N1
219 A/Solomon Islands/03/2006 (H1/SI06) HA in complex with AG11-2F01 and 16.ND.92 to
220 resolutions of 2.89 Å and 2.82 Å, respectively (**Figure 5A-E and Table S6**). Contrary to our
221 hypothesis, the cryo-EM structures revealed very different binding modes between the two
222 antibodies. While AG11-2F01 bound to HA stem horizontally, 16.ND.92 had a downward
223 approaching angle towards HA (**Figure 5A**). Relatedly, the epitope of 16.ND.92 shifted slight
224 upward compared to that of AG11-2F01 (**Figure 5B**).
225
226 Although both 16.ND.92 and AG11-2F01 were encoded by IGKV1-5, their light chains
227 interacted with the HA stem differently. For example, V_L S30 of AG11-2F01 H-bonded with
228 HA2 Q38, whereas that of 16.ND.92 H-bonded with HA1 K32 (**Figure 5C**). Similarly, despite
229 sharing an FG[V/L] motif in their IGHD3-3-encoded regions, 16.ND.92 and AG11-2F01 used
230 this motif to interact with different parts of the HA stem (**Figure 5D**). For the FGL motif in
231 AG11-2F01, V_H F100 inserted into a hydrophobic pocket in the HA stem centering at HA2
232 I48, whereas V_H L100b inserted into a lower pocket centering at HA2 W21. By contrast, this
233 lower pocket was occupied by the V_H F100a of the FGV motif in 16.ND.92. The paratope of

16.ND.92 also involved IGHD3-3-encoded V_H V100, I100e, and I100f, allowing its CDR H3 to bind to upper pockets in the HA stem that were not engaged by AG11-2F01 (**Figure 5D**). Together, our structural analyses showed that AG11-2F01 and 16.ND.92 formed distinct molecular interactions with HA stem.

16.ND.92 utilizes IGHD3-3 in a unique manner for binding to HA stem

Previous studies have determined the structures of several HA stem antibodies with an FG[V/L/I] motif in the CDR H3 that was encoded by reading frame +3 of IGHD3-3, including MEDI8852, 56.a.09, 54-1G05, 39.29, PN-SIA28, and 429 B01[7,9,31–34]. These six HA stem antibodies used either IGHV6-1 or IGHV3-30, unlike AG11-2F01 and 16.ND.92, which used IGHV4-38-2 and IGHV3-74, respectively. Nevertheless, the CDR H3 conformation of AG11-2F01 resembled that of MEDI8852, 56.a.09, 54-1G05, 39.29, PN-SIA28, and 429 B01 (**Figure 5E**). Moreover, the IGHD3-3-encoded FG[V/L/I] motifs of these seven antibodies bound to the HA stem in a similar fashion (**Figure 5E**). In comparison, the CDR H3 conformation of 16.ND.92 was different due to more extensive involvement of IGHD3-3 in binding (**Figure 5D-E**).

The unique usage of IGHD3-3 for binding enables 16.ND.92 V_H to interact with the HA stem exclusively through CDR H3, whereas the V_H paratopes of other IGHD3-3 HA stem antibodies involved non-CDR H3 regions (**Figure 5F and Table S7**). Similarly, IGHD3-3 accounted for 98.6% of the buried surface area of the 16.ND.92 V_H paratope, but 38% to 63% of the V_H paratopes of other IGHD3-3 HA stem antibodies (**Figure 5G and Table S7**). These observations not only substantiated that reading frame +3 of IGHD3-3 was a recurring sequence feature of HA stem antibodies, but also demonstrated that it could pair with diverse IGHV genes and interact with HA stem via different binding modes.

AG11-2F01 and 16.ND.92 are neutralizing antibodies with *in vivo* protection activity

Given the different binding modes of AG11-2F01 and 16.ND.92, we further aimed to compare their binding breath, *in vitro* neutralization, and *in vivo* protection activity. ELISA showed that both AG11-2F01 and 16.ND.92 bound to all H1 and H5 HAs tested (**Figure 6A and Figure S14)**, Microneutralization assay against six H1N1 strains further revealed their neutralizing activity (**Figure 6B**). Both AG11-2F01 and 16.ND.92 also protected mice against a lethal challenge of H1N1 A/Puerto Rico/8/1934 (PR8), based on the weight loss profiles (**Figure 6C-D**), survival analyses (**Figure 6E-F**), and lung viral titers at day 3 post-infection (**Figure 6G-H**). Nonetheless, our results indicated that the *in vivo* therapeutic protection activity of 16.ND.92 was stronger than AG11-2F01. While only 20% (1/5) of the mice therapeutically treated with AG11-2F01 survived (**Figure 6E**), 80% (4/5) of the mice therapeutically treated with 16.ND.92 survived (**Figure 6F**). Additionally, at day 3 post-infection, lung viral titers of mice therapeutically treated with 16.ND.92 were ~15-fold lower than those treated with AG11-2F01 (**Figure 6G-H**). Notably, 16.ND.92 had comparable, if not weaker, *in vitro* neutralizing activity than AG11-2F01 against PR8 (**Figure 6B**). Consequently, the stronger *in vivo* protection activity of 16.ND.92 against PR8 may at least be partly attributed to its more downward approaching angle to the HA stem (**Figure 5A**), which could help position the Fc region closer to effector cells.

DISCUSSION

Antibody discovery has led to significant advancements on many fronts, including antibody-based therapeutics as well as vaccine designs[11,35–38]. Discovery of natively paired antibody sequences has been hugely accelerated by scBCR-seq in the past few years[1]. However, going from sequence information to specificity characterization remains a major bottleneck in antibody discovery. In this study, we presented oPool^{+} display, an experimental platform that allows specificity characterization of antibodies with defined sequences in a highly parallel fashion. Importantly, oPool^{+} display was more cost-efficient (~$30 per antibody) and faster (~3-5 days) than the conventional methods that require cloning and recombinant expression of individual antibodies (~$200-350 per antibody, weeks to months) (**Table S8**). As a proof-

of-concept, we applied oPool+ display to delineate the binding specificity of hundreds of HA antibodies that were left uncharacterized in the literature. Follow-up analysis of AG11-2F01 and 16.ND.92 further revealed the versatility of IGHD3-3 in targeting the HA stem.

A key feature of oPool+ display is its relatively simple protocol. A previous study has shown that the throughput for screening antibodies with defined sequences can be increased by using liquid handlers to express individual antibodies one by one[39]. In comparison, oPool+ display uses a near one-pot strategy for antibody library synthesis and screening. As suggested by our results, one 96-well plate PCR can allow rapid assembly of library up to ~20,000 natively paired antibodies. With current display technologies, such as mRNA display, screening of the library against 10 to 20 antigens can be done by one person in hours. Moreover, it only requires standard benchtop equipment commonly found in a regular molecular biology lab. In addition, the constructed library can be stored long-term as DNA for future use when new antigens of interest emerge, such as novel HA variants or subtypes. The library can also be expanded by merging with additional oligo pools when new panels of antibodies are discovered. Therefore, oPool+ display not only bridges the gap between scBCR-seq and protein display technologies through massively parallel reconstruction of sequenced antibodies, but also provide more flexibility of the current antibody discovery pipelines. After the natively paired antibody sequences are obtained from scBCR-seq, oPool+ display can be applied to validate and characterize the specificity of a large panel of antibody candidates at any time. The synergy between oPool+ display and scBCR-seq can streamline the transition from antibody discovery to antibody characterization.

Previous studies have shown that IGHV6-1 and IGHV3-30 HA stem antibodies often utilize IGHD3-3-encoded FG[V/L/I] motif for binding to HA stem[7,9,31–34]. As demonstrated by our work here, IGHD3-3-encoded FG[V/L/I] motif can also pair with other IGHV genes to target HA stem, substantiating that it is an IGHV-independent recurring sequence feature of HA stem antibodies. Our results further revealed that IGHD3-3 can engage the HA stem via

different binding modes. These observations are comparable to those of IGHD3-9, which is utilized by HA stem antibodies with various IGHV genes and can bind to HA stem in two different reading frames[14]. Similarly, recent studies have identified IGHD3-22 as an IGHV-independent recurring sequence feature of antibodies that target a conserved site on SARS-CoV-2 spike[40,41]. Although antibody sequence analysis typically focuses on IGHV genes, the contribution of IGHD genes to antibody responses should not be overlooked since emerging evidence suggests that it might be more important than previously thought.

Although this study focused on influenza HA stem as a proof-of-concept, oPool$^+$ display can be generalized to any antigens of interest as long as they can be recombinantly purified. Importantly, oPool$^+$ display can be leveraged for epitope mapping, given that it enables competition screening. Such application will be particularly valuable for antigens that have largely unknown antigenicity but have several antibodies with known epitopes, such as those from emerging pathogens[42,43]. Furthermore, the capability of constructing custom-made antibody libraries means that oPool$^+$ display has the potential to benefit the development of machine learning models for antibody engineering, specificity prediction, and *de novo* design, as a major throughput bottleneck still exists in experimental validation[16,44–46]. We envision that prediction results from these models can be rapidly validated by oPool$^+$ display, which will in turn facilitate iterative refinement of the models for more advanced applications.

We acknowledge that oPool$^+$ display has some limitations. First, oPool$^+$ display requires antibodies to be presented as scFvs, which may lose functionality compared to its Fab counterpart[47–49]. Second, antibodies with a fast off-rate may result in false negatives in oPool$^+$ display, since it depends on monovalent binding. Inadequate wash during selection could also partially explain the false positive hits in our results. Nonetheless, a few solutions can be adopted in future studies. Performing multiple rounds of mRNA display selection, or replacing it with other protein display technologies that support multivalent binding, such as yeast display and phage display, can further reduce false negative rate[50,51]. In addition, a

more stringent wash protocol can potentially reduce false positive rate. As the length of oligo pool synthesis continues to improve, the cost and complexity of oPool$^+$ display will further decrease. Overall, we believe that oPool$^+$ display represents a starting point for the future advancement of high-throughput approaches to characterize antibodies.

MATERIALS AND METHODS

Selection of HA antibodies for paired antibody library synthesis

Members of the natively paired antibody library were selected from a previously curated dataset containing 5,561 human monoclonal antibodies to influenza HA from 60 research publications and three patents[16]. Filters were applied to exclude antibodies that 1) had incomplete sequence information, 2) utilized germline genes that were regarded as recurring sequence features of HA stem antibodies, namely IGHV1-69, IGHV6-1, IGHV1-18 and IGHD3-9[7,12–14], and 3) were members of known HA stem antibody clonotypes. This resulted in 292 antibody sequences from 7 publications[7,17–19,23,52,53]. Three HA stem antibodies, namely 31.a.55, AG11-2F01, and 042-100809-2F04, as well as 30 HA head antibodies were randomly selected as positive and negative controls[6,7,15,17–25]. Of note, both AG11-2F01 and 042-100809-2F04 were not previously labeled as an HA stem antibody in the curated dataset[16]. Through literature search, AG11-2F01 was found to compete with CR9114[10], which is an HA stem antibody, for binding to H1[17], while 042-100809-2F04 was found to bind to group 2 HA stem domain[54].

Computational design of the oligo pool sequences for assembly

A summary of the computational design pipeline is described below and summarized in **Figure S1**.

Sequence preparation

Selected antibody sequences were first annotated using abYsis[55]. Any missing nucleotides at the 5' and/or 3' ends were then filled in using the sequences from the IGHV and IGHJ genes that had the highest identity with the given antibody.

Codon randomization and pool assignment of the antibodies

To decrease undesired assembly during antibody library synthesis, codon randomization of each selected antibody sequence was first performed to reduce nucleotide sequence similarity among different antibodies. For a given amino acid, codon usages <15% in *Escherichia coli* were removed from consideration to prevent low translation efficiency during RNA display. For 325 antibodies, total of 2 million randomized sequences were generated to maximize downstream sequence differentiation. All antibody sequences were then split into 8 segments, followed by clustering using CD-HIT[56]. The clusters were generated using the criterion of 70% sequence identity (at least 30% differences between each cluster). The antibody sequences were then reconstructed by selecting necessary segments from different clusters, followed by removing the used clusters. Such reconstruction was repeated until a complete pool (total of 25 antibody sequences) had been reassembled. The deleted clusters were then added back with the reassembled antibody sequences removed. The process was then iterated to generate the remaining pools.

Selection of overlap regions and generation of the final oligo pools

Upon the pool assignment of antibodies, the ideal overlap regions were searched over CDR L3, H1, and H3 of each antibody sequence. Six 30-nucleotide long sequences were extracted from each region through frame shifting, then aligned to the complete antibody sequences in the corresponding pool using BLAST+[57]. For each antibody, the overlap sequences that are least similar to other antibodies in the pool were selected. The antibody sequences were then split at the overlap region, followed by the addition of universal adaptor regions at fragments encoding the N-terminal and C-terminal of the antibodies, leading to the generation of the final oligo pools.

Overlap PCR assembly of the natively paired antibody library

A total of 13 oligo pools were synthesized (Integrated DNA Technologies). The lengths of oligos ranged from around 180 to 330 nucleotides. Each oligo pool contained 100 oligos resuspended in 200 µL water. An assembly PCR was set up for each oligo pool using 1,600 ng of oligos as input. The assembly was performed using KAPA HiFi HotStart ReadyMix (Roche) and a Mastercycler nexus GX2 (Eppendorf). PCR was set up in the absence of primers. From cycles 1-40, PCR was performed with minimal ramp rate (0.1°C/s) in between the denaturing (98°C, 20 s) and annealing steps (62°C, 15 s) to reduce erroneous annealing events. After cycle 40, a universal forward primer 5'-TTC TAA TAC GAC TCA CTA TAG GGA CAA TTA CTA AAG GAG TAT CC-3' and a universal reverse primer 5'-GGA GCC GCT ACC CTT ATC GTC GTC ATC CTT GTA ATC GGA TCC T-3' were added to the PCR. The underlined region in the forward primer sequence is the T7 promoter, whereas the underlined region in the reverse primer sequence encodes a FLAG tag. Subsequently, another 15 cycles of PCR were performed to amplify the assembled product. The final PCR product was purified using a Monarch Gel Extraction Kit (New England Biolabs). Two replicates of the assembly were performed.

Preparation of the biotinylated H1 stem and H3 stem constructs

The H1 stem (mini-HA #4900)[29], H3 stem (H3ssF)[30], as well as the seven HA ectodomain constructs were cloned into a customized baculovirus transfer vector. Both constructs contained a N-terminal gp67 signal peptide at the N-terminus as well as a BirA biotinylation site, a thrombin cleavage site, a trimerization domain and a 6×His-tag at the C-terminus. Recombinant bacmid DNA that carried the H1 stem construct or H3 stem construct was generated using the Bac-to-Bac system (Thermo Fisher Scientific) per manufacturer's instructions. Baculovirus was generated by transfecting the purified bacmid DNA into adherent Sf9 cells using Cellfectin reagent (Thermo Fisher Scientific) per manufacturer's

instructions. The baculovirus was further amplified by passaging in adherent Sf9 cells at a multiplicity of infection (MOI) of 1.

Recombinant HA constructs were then expressed using 1L of suspension Sf9 cells at an MOI of 1. At day 3 post-infection, Sf9 cells were pelleted by centrifugation at 4,000 ×g for 25 min. Soluble recombinant HA constructs were purified from the supernatant by affinity chromatography using Ni Sepharose excel resin (Cytiva) and then size exclusion chromatography using a HiLoad 16/100 Superdex 200 prep grade column (Cytiva) in 20 mM Tris-HCl at pH 8.0, and 100 mM NaCl. The purified protein was concentrated by an Amicon spin filter (Millipore Sigma) and filtered by a 0.22 mm centrifuge Tube Filter (Costar). The purified HA constructs were then biotinylated using a Biotin-Protein Ligase-BIRA kit (Avidity) according to the manufacturer's instructions. The biotinylated proteins were then purified again through size exclusion chromatography as described above. The A280 absorbance values were measured using a Nanodrop One (Thermo Fisher Scientific) to quantify the protein concentration.

Antibody screening using mRNA display

The mRNA display was performed based on the protocols provided by previous studies[27,28,58] with slight modifications.

Generation of the puromycin-conjugated mRNA templates

The DNA library was first transcribed by a MEGAscript T7 Transcription Kit (Thermo Fisher Scientific) and purified by a MEGAclear Transcription Clean-Up Kit (Thermo Fisher Scientific) according to manufacturer's instructions. Ligation was performed using 1 nmol of the mRNA product, 1.1 nmol of the splint oligo (5'-TTT TTT TTT TTT GGA GCC GCT ACC-3'), and 1.2 nmol of the puromycin linker (5'-/5Phos/-d(A)21-(C_9)3-d(ACC)-puromycin-3') by the T4 DNA ligase (New England Biolabs) in a 100 µL reaction for 1 hour at room temperature, followed by Lambda exonuclease (New England Biolabs) digestion for 30 mins at 37°C. The

454 puromycin-conjugated mRNA product was purified using a Dynabeads mRNA DIRECT
455 Purification Kit (Thermo Fisher Scientific), aliquoted, and stored at -20°C until used.
456
457 *Preparation of the mRNA-scFv fusion library*
458 The puromycin-conjugated mRNA templates were translated using a PURExpress In Vitro
459 Protein Synthesis Kit (New England Biolabs) with the addition of PURExpress Disulfide
460 Bond Enhancer (New England Biolabs) for 1 hour at 37°C. The reaction was then incubated
461 with 500 mM KCl and 60 mM $MgCl_2$ for at least 30 mins at room temperature to promote
462 fusion between the translated scFv and puromycin. EDTA was then added to dissociate
463 ribosomes. The full-length mRNA-scFv product was then purified using Anti-FLAG M2
464 Magnetic Beads (Millipore Sigma) followed by elution using 3× FLAG peptides (GlpBio).
465 Subsequently, the purified mRNA-scFv product was reverse transcribed using SuperScript
466 IV reverse transcriptase (Thermo Fisher Scientific). The cDNA/mRNA-scFv product was
467 referred as the “pre-selection library”.
468
469 *Preparation of the magnetic beads coated with biotinylated HAs*
470 Biotinylated HA constructs were coated onto the Dynabeads M280-straptavidin (Thermo
471 Fisher Scientific) according to the manufacturer’s instruction. Briefly, 150 pmol of biotinylated
472 proteins were incubated with 50 µL of the beads for 30 mins to 1 hour at room temperature
473 with gentle rotation. The beads were then washed with TBST (20 mM Tris-HCl at pH 7.5,
474 100mM NaCl, and 0.025% Tween-20) five times using the DynaMag-2 magnetic holder
475 (Thermo Fisher Scientific) and then resuspended to the original volume.
476
477 *Antibody selection against HAs*
478 Selection of antibodies against HA constructs were carried out in parallel. Briefly, the pre-
479 selection library was mixed with 25 µL of beads coated with each HAs and incubated for 1
480 hour at room temperature with gentle rotation. After incubation, the beads were washed

thrice with 400 µL TBST. The beads were then resuspended in water. These samples were referred as the “post-selection libraries”.

Antibody selection against HAs with CR9114 competition

The CR9114 competition screen was performed as describe above with the addition of a CR9114 blocking step prior to the selection. In brief, 25 µL beads coated with HAs were blocked with 2uM CR9114 IgG[10], followed by the addition of 7.5uL of input library and incubation for 1 hour at room temperature with gentle rotation. After incubation, the beads were washed thrice with 400 µL TBST. The beads were then resuspended in water. These samples were referred as the “post-selection libraries”.

Next-generation sequencing of the scFv library

The pre-selection libraries, post-selection libraries, and the small pool assemblies selected for quality control were amplified using PrimeSTAR Max DNA Polymerase (Takara Bio) per manufacturer’s instruction with the following primers (5’-GTA AAA CGA CGG CCA GTT TCA GGG GAC AAT TAC TAA AGG AGT ATC C-3’ and 5’- CAG GAA ACA GCT ATG ACC CAC TCG TCA TCC TTG TAA TCG GAT CCT CCG GA-3’. The PCR product was purified using a Monarch Gel Extraction Kit (New England Biolabs). A second round of PCR was carried out to add the adapter sequence and index to the amplicons (**Table S9**). The final PCR products were sequenced on one SMRTcell 8M on a PacBio Revio system using the CCS sequencing mode and a 30-hour movie time.

Analysis of next-generation sequencing data

Circular consensus sequences (CCSs) were generated from the raw subreads using SMRTLink v13.0, setting the parameters to require 99.9% accuracy and a minimum of 3 passes. CSSs in FASTQ format were parsed using the SeqIO module in BioPython[59] and filtered based on the base calling quality score, where any read with more than five nucleotides of phred quality score <40 were removed. The adapter sequences were then

identified on each read and trimmed from the scFv sequences. Reads that did not have the complete adapter sequences were also removed. The filtered reads were then aligned to the reference scFv sequences and classified into three categories: 1) natively paired scFvs with no mutation, 2) natively paired scFvs with mutation, 3) others (non-natively paired scFvs and incomplete assemblies). Only the reads encoding natively paired scFvs with no mutation were used for downstream analysis. Frequency (*F*) of a scFv *i* a given replicate *k* of a given antigen *s* was computed for each replicate as follows:

$$F_{i,k,s} = \frac{readcount_{i,k,s}+1}{\sum_s(readcount_{i,k,s}+1)} \quad (1)$$

A pseudocount of 1 was added to each mutant to avoid division by zero in subsequent steps. We then calculated the enrichment (*E*) of a scFv *i* of a given replicate *k* of a given antigen *s* after the mRNA display selection as follows:

$$E_{i,k,s} = \frac{F_{post-selection,i,k,s}}{F_{pre-selection,i,k}} \quad (2)$$

We calculated the mean enrichment of a scFv *i* of a given antigen *s* over two replicates, then inferred the binding score (*BS*) of a scFv *i* of a given antigen *s* using robust scaling:

$$BS_{i,s} = \frac{E_{i,s}-median(E)}{IQR(E)} \quad (3)$$

Where *median(E)* represents the median of a given dataset, *IQR(E)* representing the interquartile range of a given dataset. Custom cutoffs were set for each screen to determine hits (**Table S10**). For a given antigen *s*, the CR9114 competition index (*CI*) of a scFv *i* was computed as below:

$$CI_{i,s} = \log_{10} \frac{E_{HA\ screen\ without\ CR9114,i,s}}{E_{HA\ screen\ with\ CR9114,i,s}} \quad (4)$$

Expression and purification of Fabs and IgGs

Heavy and light chains of the antibodies were cloned into a phCMV3 vector with a mouse immunoglobulin kappa signal peptide in human IgG1 Fc or Fab format. Plasmids encoding the heavy and light chains of antibodies were transfected into Expi293F cells using an ExpiFectamine 293 transfection kit (Gibco) in a 2:1 mass ratio for IgG or a 1:1 mass ratio for

Fab following the manufacturer's protocol. Supernatant was harvested at 6 days post-transfection and centrifuged at 4,000 ×g for 30 mins at 4°C to remove cells and debris. The supernatant was subsequently clarified using a polyethersulfone membrane filter with a 0.22 mm pore size (Millipore). Antibodies were first purified by CaptureSelect CH1-XL beads (Thermo Fisher Scientific). Then, the antibodies were further purified by size exclusion chromatography using a HiLoad 16/100 Superdex 200 prep grade column (Cytiva) in 1× PBS. The A280 were measured using the Nanodrop One (Thermo Fisher Scientific) to calculate the sample concentration. Antibodies were stored at 4°C until used.

Expression and purification of FLAG-tagged CR9114 scFv

CR9114 scFv nucleotide sequence with a pelB secretion peptide at the N-terminal and a FLAG-tag (DYKDDDK) followed by a stop codon at the C-terminal were synthesized (Integrated DNA Technologies) and ligated into a pET-28a plasmid vector backbone using NEBuilder HiFi DNA Assembly Master Mix (New England Biolabs). The ligated product was then transformed into DH5α competent cells (Thermo Fisher Scientific), and the plasmids were extracted using a QIAprep Spin Miniprep Kit (Qiagen). The plasmids were then transformed into BL21(DE3) competent cells (Thermo Fisher Scientific), followed by overnight growth at 37°C, 225 rpm shaking. 100 mL LB culture (Fisher Scientific) were inoculated at 1:500 ratio using the overnight culture and shaken at 37°C, 225 rpm. Once the OD_{600} reached approximately 0.6, IPTG (1 mM final concentration) was added to induce protein expression for 16 hours at 30°C, 200 rpm.

The overnight culture was centrifuged at 4,500 ×g, 4°C for 1 hour to remove the supernatant. The pellet was resuspended using 2 mL of ice-cold 1× TES buffer (200 mM Tris-HCl at pH 8.0, 0.65 mM EDTA, and 0.5 M sucrose). The resuspended mixture was incubated at 4°C for 2 hours with gentle shaking. 5 mL of ice-cold 0.25× TES buffer was then added, followed by incubation at 4°C overnight. The mixture was centrifuged at 4,500 ×g, 4°C for 1 hour to remove the pellet. The supernatant was subsequently clarified using a polyethersulfone membrane filter with a 0.22 mm pore size (Millipore) and purified using ANTI-FLAG M2

Affinity Gel (Millipore-Sigma) per manufacturer's instructions. The A280 was measured using the Nanodrop One (Thermo Fisher) to calculate the sample concentration.

Expression, purification, and quantitation of selected scFvs for validation

Nucleotide sequences of selected scFvs with a T7 promoter at the N-terminal and a FLAG-tag (DYKDDDK) followed by a stop codon at the C-terminal were synthesized (Integrated DNA Technologies) and amplified by PCR using Prime STAR Max DNA polymerase (Takara Bio). The PCR product was purified using a PureLink PCR purification kit (Thermo Fisher Scientific) and used as the template for *in vitro* translation using a PURExpress In Vitro Protein Synthesis Kit (New England Biolabs) with the addition of PURExpress Disulfide Bond Enhancer (New England Biolabs). The translated scFvs were then reverse purified using Pierce High-Capacity Ni-IMAC magnetic beads (Thermo Fisher Scientific) per manufacturer's instructions to remove all His-tagged translation kit components.

To measure the concentration of the purified scFv, quantitation assays were performed by biolayer interferometry (BLI) using an Octet Red instrument (Sartorius). Briefly, rat anti-FLAG tag monoclonal antibody (L5) (Thermo Fisher Scientific) at 5 µg/mL in 1× kinetics buffer (1× PBS at pH 7.4, and 0.002% v/v Tween 20) were loaded onto ProG biosensors (Sartorius), then incubated with the 40× diluted scFv sample (5 µL of sample added to 195 µL of 1× kinetics buffer). The standard curve was generated via 2-fold serial dilutions using FLAG-tagged CR9114 scFv. The assay consisted of five steps: (1) baseline: 60 s with 1× kinetics buffer; (2) antibody capture: 180 s with rat anti-FLAG antibody; (3) baseline: 60 s with 1× kinetics buffer; (4) binding rate measurement: 120 s with standard and scFv samples; and (5) regeneration: 5s in regeneration buffer (0.1 M Glycine at pH 3.0) followed by 5 s in neutralization buffer (1 M Tris-HCl at pH 7.5), repeated 3 times. The data were analyzed using Octet analysis software 9.0, where the first 30 s of the binding rate measurement were used for final quantitation.

Validation of oPool^{+} display via biolayer interferometry

The binding assay was performed by biolayer interferometry (BLI) using an Octet Red instrument (Sartorius). 1× kinetics buffer (1× PBS at pH 7.4, and 0.002% v/v Tween 20) were used for all experiments. Details of each experiment were described below:

Systematic binding validation

SA biosensors and Fab2G biosensors (Sartorius) were used for to validate binding of selected antibodies against the nine HA constructs. HA or Fab constructs at 20 μg/mL in 1× kinetics buffer were loaded onto the biosensors and incubated with 10 μg/mL Fabs/HAs. Measurements with NA and each Fab were also taken to serve as the baseline. The assay consisted of five steps: (1) baseline: 60 s with 1× kinetics buffer; (2) loading: 60 s with biotinylated HA or Fab; (3) baseline: 60 s with 1× kinetics buffer; (4) association: 60 s with Fab or HA samples; and (5) dissociation: 60 s with 1× kinetics buffer. The binding response during the association step were recorded.

Fab K_D measurement

Biotinylated H1 or H3 stem construct at 0.5 μM in 1× kinetics buffer was loaded onto SA biosensors (Sartorius) and incubated with 33 nM, 100 nM, and 300 nM of purified Fabs. The assay consisted of five steps: (1) baseline: 60 s with 1× kinetics buffer; (2) loading: 120 s with biotinylated HA stem domains; (3) baseline: 60 s with 1× kinetics buffer; (4) association: 120 s with Fab samples; and (5) dissociation: 120 s with 1× kinetics buffer. For estimating the exact K_D, a 1:1 binding model was used.

scFv K_D measurement

Biotinylated H1 or H3 stem construct at 0.5 μM in 1× kinetics buffer was loaded onto SA biosensors (Sartorius) and incubated with 9× dilution (20 μL of sample added to 160uL of 1× kinetics buffer) and 18× dilution (10 μL of sample added to 170 μL of 1× kinetics buffer) of the purified scFv sample. The assay consisted of five steps: (1) baseline: 60 s with 1× kinetics buffer; (2) loading: 180 s with biotinylated HA stem domains; (3) baseline: 60 s with

1× kinetics buffer; (4) association: 120 s with Fab samples; and (5) dissociation: 120 s with 1× kinetics buffer. For estimating the exact K_D, a 1:1 binding model was used.

CR9114 competition assay

SA biosensors and NTA biosensors (Sartorius) were used for to validate CR9114 competition of selected antibodies. HA constructs at 20 µg/mL in 1× kinetics buffer were first loaded onto the biosensors, then incubated with 20 µg/mL CR9114 Fab until saturation in binding, immediately followed by incubation with the selected Fabs. A no-CR9114 control experiment was performed concurrently for each Fab-antigen pair. The assay consisted of five steps: (1) baseline: 60 s with 1× kinetics buffer; (2) loading: 480 s with HAs; (3) baseline: 60 s with 1× kinetics buffer; (4) first association: 180 s with CR9114 Fab or 1× kinetics buffer; and (5) second association: 120 s with 10 µg/mL selected Fabs. Of note, competition assays of SI06 with 009-10-1G06, 045-09-1G05, 009-10-2F01, and 051-10-2B05 were done in the reverse order, where the first association consist of 900 s incubation with the selected Fabs, followed by 120 s second association with 10 µg/mL CR9114 Fab. The binding response of the first 60 s in step (5) were recorded, and the CR9114 competition % of a given antibody *i* against antigen *s* were calculated as below:

$$CR9114\ competition\ \%_{i,s} = \left(1 - \frac{Response_{w/CR9114\ Fab,i,s}}{Response_{w/oCR9114\ Fab,i,s}}\right) \times 100\% \quad (5)$$

Expression and purification of HA ectodomains

The HA ectodomains of H1N1 A/Puerto Rico/8/1934, H1N1 A/Beijing/262/1995, H1N1 A/Brisbane/02/2018 were cloned, expressed, and purified as mentioned above for the HA constructs used for screening. The HA ectodomains of H1N1 A/California/04/2009 (NR-15749), H5N1 A/bald eagle/Florida/W22-134-OP/2022 (NR-59476), H5N2 A/snow goose/Missouri/CC15-84A/2015 (NR-50651), and H5N8 A/northern pintail/WA/40964/2014 (NR-50174) were obtained from BEI Resources (https://www.beiresources.org/). The HA ectodomains of H1N1 A/USSR/90/1977 and H1N1 A/Taiwan/01/1986 were purchased from SinoBiological.

649

650 **Cryo-EM sample preparation, data collection, and data processing**

651 *AG11-2F01 Fab in complex with H1/SI06 HA*

652 The AG11-2F01 Fab was incubated with H1/SI06 HA on ice overnight followed by size
653 exclusion chromatography. The peak fraction of the Fab-HA complex was concentrated to
654 around 1 mg/mL for cryo-EM sample preparation. Cryo-EM grids were prepared using a
655 Vitrobot Mark IV (Thermo Fisher Scientific). 3.5 µL of the sample was applied to a 300-mesh
656 Quantifoil R1.2/1.3 Cu grid pretreated with glow-discharge. Excess liquid was blotted away
657 using filter paper with blotting force -5 and blotting time 3 s. The grid was then flash frozen in
658 liquid ethane. Movies were then collected on a Titan Krios microscope equipped with Gatan
659 BioQuantum K3 imaging filter and camera (Thermo Fisher Scientific). Images were recorded
660 at 130,000× magnification, corresponding to a pixel size of 0.33 Å/pixel at super-resolution
661 mode of the camera. A defocus range of -0.8 µm to -1.5 µm was set. A total dose of 50 $e^-/Å^2$
662 of each exposure was fractionated into 50 frames. Both untilted and 30-degree-tilted data
663 were collected and combined to alleviate the preferred orientation problem of the sample.

664

665 CryoSPARC[60] was used to process the cryo-EM data. For model building, ABodyBuilder[61]
666 was used to generate an initial model for AG11-2F01 Fab. This model, together with the
667 model of H1/SI06 HA (PDB 6FYT)[62], was fitted into the cryo-EM density map using UCSF
668 Chimera[63]. The model was manually adjusted in Coot[64] and refined with Phenix real-space
669 refinement program[65]. This process was iterated for several cycles until no significant
670 improvement of the model was observed.

671

672 *16.ND.92 Fab in complex with H1/SI06 HA*

673 The 16.ND.92 Fab was incubated with H1/SI06 HA and FISW84 Fab, a known HA anchor
674 antibody[66], on ice overnight followed by size exclusion chromatography. The peak fraction of
675 the Fab-HA complex was concentrated to around 3 mg/mL for cryo-EM sample preparation.
676 0.1% (w/v) of n-octyl-ß-D-glucoside was added to reduce orientation bias. Cryo-EM grids

were prepared using a Vitrobot Mark IV (Thermo Fisher Scientific). 3 µL of the sample was applied to a 400-mesh Quantifoil R1.2/1.3 Cu grid pretreated with glow-discharge. Excess liquid was blotted away using filter paper with blotting force 0 and blotting time 3 s. The grid was then flash frozen in liquid ethane. Movies were then collected on a Titan Krios microscope equipped with Gatan BioQuantum K3 imaging filter and camera (Thermo Fisher Scientific). Images were recorded at 81,000× magnification, corresponding to a pixel size of 0.53 Å/pixel at super-resolution mode of the camera. A defocus range of -0.5 µm to -5 µm was set. A total dose of 57.35 $e^-/Å^2$ of each exposure was fractionated into 40 frames.

CryoSPARC[60] was used to process the cryo-EM data. DeepEMhancer[67] was used to generate the sharpened density map for downstream model building. For model building, IgFold[68] was used to generate an initial model for 16.ND.92 Fab. This model, together with the model of H1/SI06 HA (PDB 6FYT)[62], was fitted into the cryo-EM density map using Phenix DockinMap module[69]. The models were manually adjusted in Coot[64] and refined with Phenix real-space refinement program[65]. This process was iterated for several cycles until no significant improvement of the model was observed.

Structural analysis of HA-antibody complexes

Buried surface areas upon binding and paratope residues of AG11-2F01, 16.ND.92, MEDI8852 (PDB 5JW4), 56.a.09 (PDB 5K9J), 54-1G05 (PDB 6WIZ), PN-SIA28 (PDB 8GV5), 39.29 (PDB 4KVN), and 429 B01 (PDB 6NZ7)[7,9,31–34] were analyzed using PDBePISA[70]. The CDRH3 region and IGHD 3-3 usage of each antibody was annotated using IgBLAST[71]. The molecular interactions of AG11-2F01 and 16.ND.92 in complex with H1/SI06 HA were analyzed and visualized using PyMOL (Schrödinger).

Enzyme-linked immunosorbent assay (ELISA)

Nunc MaxiSorp ELISA plates (Thermo Fisher Scientific) were coated overnight at 4°C with 100 µL of recombinant proteins at 1 µg/mL in 1× PBS. The next day, plates were washed

thrice with 1× PBS containing 0.05% Tween 20 and blocked with 200 µl of 5% non-fat milk in 1× PBS for 2 hours at room temperature. For systematic validation of oPool^{+} display, 10 µg/mL of monoclonal antibodies were added to the plates, and incubated for 2 hours at 37°C; for functional characterization of AG11-2F01 and 16.ND.92, monoclonal antibodies were serially diluted 10-fold starting from 100 µg/mL, added to the plates, and incubated for 2 hours at 37°C. Plates were then washed thrice and incubated with horseradish peroxidase (HRP)-conjugated goat anti-human IgG antibody (Thermo Fisher Scientific) at 1:5,000 dilution for 1 hour at 37°C. After six washes with 1× PBS containing 0.05% Tween 20, 100 µL of 1-Step TMB ELISA Substrate Solution (Thermo Fisher Scientific) was added to each well. After incubation for 10 mins, the reaction was stopped with 50 µL of 2 M H_2SO_4 solution, and absorbance values were measured at 450 nm (OD_{450}) using a BioTek Synergy HTX Multimode Reader (Agilent).

Recombinant virus construction and purification

Recombinant viruses with HA and NA segments from the indicated H1N1 strains and six internal segments from H1N1 A/Puerto Rico/8/1934 (PR8) were obtained from BEI Resources (https://www.beiresources.org/). Recombinant viruses were rescued using the eight-plasmid reverse genetics system[72]. Briefly, plasmids encoding the HA segments from H1N1 A/California/07/2009 and H1N1 A/Michigan/45/2015 along with seven plasmids encoding the other seven segments from PR8 were transfected into a co-culture of HEK293T (human embryonic kidney) cells and MDCK-SIAT1 (Madin-Darby Canine Kidney) cells at a 6:1 ratio. Supernatants were injected into 8-10 days old embryonated chicken eggs and incubated at 37°C for 48 hours. Viruses in the allantoic fluid were plaque-purified on MDCK-SIAT1 cells grown in Dulbecco's Modified Eagles Medium (Gibco) containing 10% fetal bovine serum (Gibco) and a penicillin-streptomycin mix (100 U/mL penicillin and 100 µg/mL streptomycin, Gibco). The HA sequence of each virus was confirmed by Sanger sequencing.

Microneutralization assay

For the microneutralization assay, MDCK-SIAT1 cells were seeded in 96-well plates. After reaching 100% confluency, MDCK-SIAT1 cells were washed once with 1× PBS. Minimal essential media (Gibco) containing 25 mM HEPES (Gibco) was then added to the cells. Monoclonal antibodies were serially diluted 10-fold starting from 100 µg/ml and mixed with 100 $TCID_{50}$ (median tissue culture infectious dose) of viruses at equal volume and incubated at 37°C for 1 hour. Subsequently, the mixture was inoculated into cells and incubated at 37°C for another hour. Cell supernatants were discarded and replaced with minimal essential media containing 25 mM HEPES, and 1 µg/mL TPCK-trypsin (Sigma). Plates were incubated at 37°C for 72 hours, and virus presence was detected by hemagglutination assay to determine the MN_{50} titers.

Mice

The animal experiments were performed in accordance with protocols approved by UIUC Institutional Animal Care and Use Committee (IACUC). Six-week-old female BALB/c mice (Jackson Laboratory) were used for all animal experiments.

Prophylactic and therapeutic protection experiments

Female BALB/c mice at 6 weeks old (n = 5 per group) were anesthetized with isoflurane and intranasally infected with 5× lethal dose (LD_{50}) of recombinant PR8 virus. Mice were given the indicated antibody at a dose of 5 mg/kg intraperitoneally at 4 hours before infection (prophylaxis) or 4 hours after infection (therapeutics). Weight loss was monitored daily for 14 days. The humane endpoint was defined as a weight loss of 25% from initial weight at day 0. Of note, while our BALB/c mice were not modified to facilitate interaction with human IgG1, human IgG1 could interact with mouse Fc gamma receptors[73–75].To determine the lung viral titers at day 3 post-infection, lungs of infected mice were harvested and homogenized in 1 mL of minimal essential media with 10% bovine serum albumin using a gentleMACS C Tube (Miltenyi Biotec). Subsequently, virus titers were measured by $TCID_{50}$ assay.

ACKNOWLEDGEMENTS

We thank Anders Olson, Chris Brooke, David Kranz, and Steve Sligar for helpful discussion and the Roy J. Carver Biotechnology Center at the University of Illinois at Urbana-Champaign for assistance with PacBio sequencing. We thank Kristen Flatt and the Materials Research Laboratory Central Research Facilities at the University of Illinois at Urbana-Champaign for access to cryo-EM instrumentation during the screening of the Fab-HA complexes. We are grateful to the Cryo-EM Core and the Core Facility for Advanced Research Computing at Case Western Reserve University for the access of cryo-EM instrumentation and data processing. We also thank Frank Vago and the Cryo-EM Facility at Purdue University for the access of cryo-EM instrumentation and data collection. This work is supported by National Institutes of Health R01 AI167910 (N.C.W.), DP2 AT011966 (N.C.W.), the Searle Scholars Program (N.C.W.), Howard Hughes Medical Institute Emerging Pathogens Initiative (N.C.W.), UIUC William T. and Lynn Jackson Graduate Student Fellowship (W.O.O.), UIUC Gregorio Weber Graduate Student Fellowship (W.O.O.), and Carl R. Woese Institute for Genomic Biology Postdoctoral Fellowship (H.L.).

AUTHOR CONTRIBUTIONS

W.O.O. and N.C.W. conceived and designed the study. W.O.O., H.L., W.L., Y.W., K.E.D. and N.C.W. developed the methodology. W.O.O. and L.T. assembled the library and performed mRNA display experiment. W.O.O., W.L. and N.C.W. analyzed the PacBio sequencing data. W.O.O., H.L., R.L., M.T., A.B.G. and L.A.R. expressed and purified recombinant proteins. W.O.O., Z.M., R.L., T.P., X.D., and N.C.W. performed structural analysis of the antibodies. W.O.O., H.L., D.C., and M.R.A performed functional characterization of the antibodies. X.D. and N.C.W. provided resources and support. W.O.O. H.L., W.L. and N.C.W. wrote the paper, and all authors reviewed and edited the paper.

DECLARATION OF INTERESTS

N.C.W. consults for HeliXon. The authors declare no other competing interests.

DATA & CODE AVAILABILITY

Raw sequencing data have been submitted to the NIH Short Read Archive under accession number: BioProject PRJNA1150188. Cryo-EM density maps and coordinates have been deposited to EMDB and PDB with accession numbers: EMD-46727 and EMD-45930; PDB 9DBX and 9CU7. Custom scripts as well as raw data for experimental validations have been deposited to: https://github.com/nicwulab/oPool_display.

MAIN FIGURES

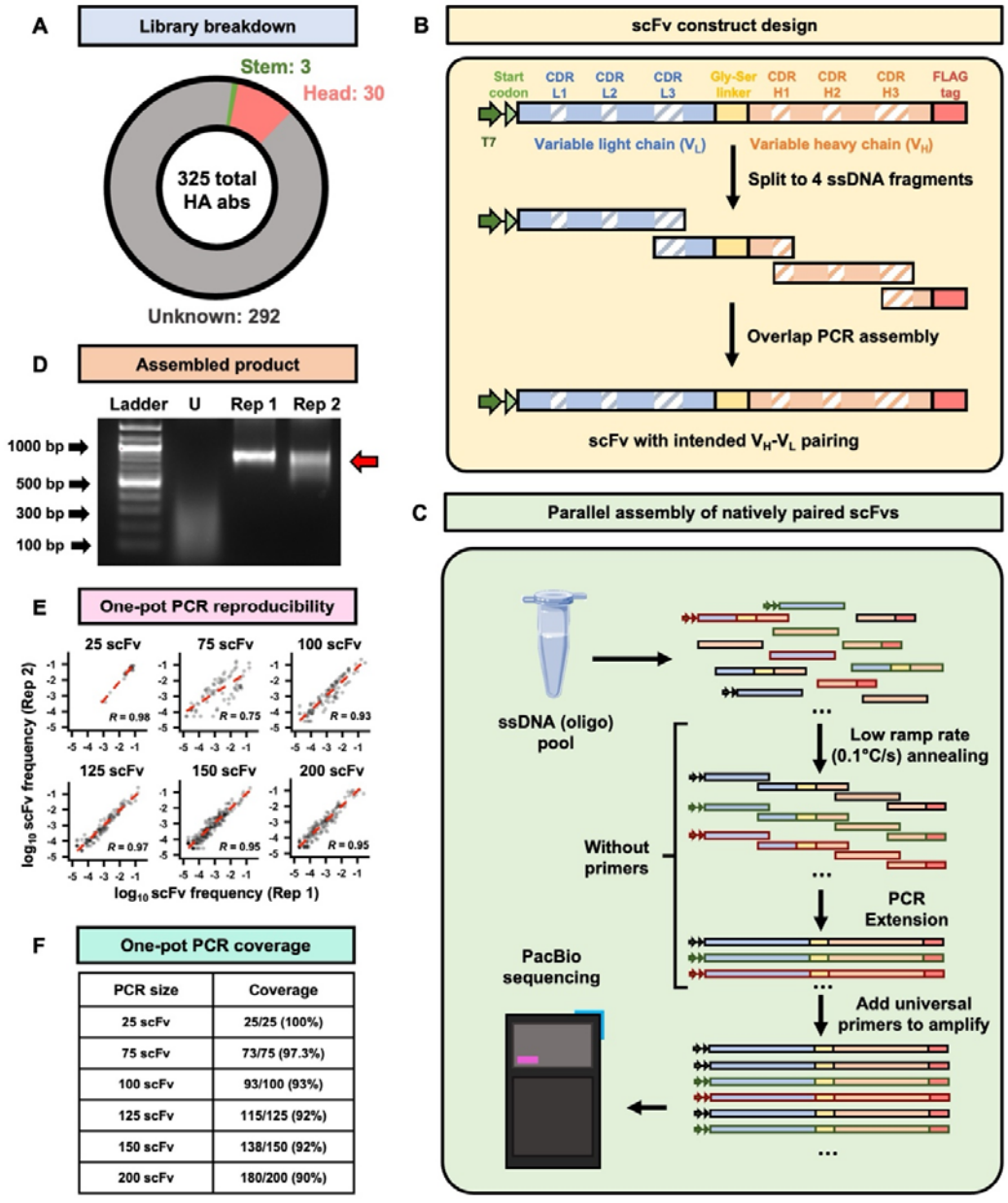

PCR size	Coverage
25 scFv	25/25 (100%)
75 scFv	73/75 (97.3%)
100 scFv	93/100 (93%)
125 scFv	115/125 (92%)
150 scFv	138/150 (92%)
200 scFv	180/200 (90%)

Figure 1. Curation and synthesis of the natively paired HA antibody library. (A) The overall breakdown of the HA antibody library. **(B)** Design of oligos for scFv assembly. Each given scFv construct contains a T7 promoter and a start codon at the N-terminal as well as a FLAG tag at the C-terminal. The scFv sequences were then split into 4 fragments at the selected CDR regions, with overlap between adjacent fragments. Through an overlap PCR, oligos of the same construct would preferably anneal to each other, ensuring the assembly of natively paired scFvs. **(C)** Synthesis of the natively paired HA antibody library.

Synthesized oligo pools containing scFv fragments were assembled via a two-stage PCR (**see Materials and Methods**). **(D)** The unassembled and assembled oligo pools were compared by agarose gel electrophoresis. "U": unassembled oligo pool. "Rep1": replicate 1. "Rep2": replicate 2. The red arrow indicates the target size (800-900 bp) for full length scFvs. **(E-F)** The reproducibility **(E)** and coverage **(F)** of the scFv assembly using varying numbers of scFv per PCR, ranging from 25 to 200. The Pearson correlation coefficient (*R*) of the occurrence frequencies of individual scFvs between the two replicates were indicated. Micro-tube icon by Servier https://smart.servier.com/ is licensed under CC-BY 3.0 Unported, available via Bio Icons.

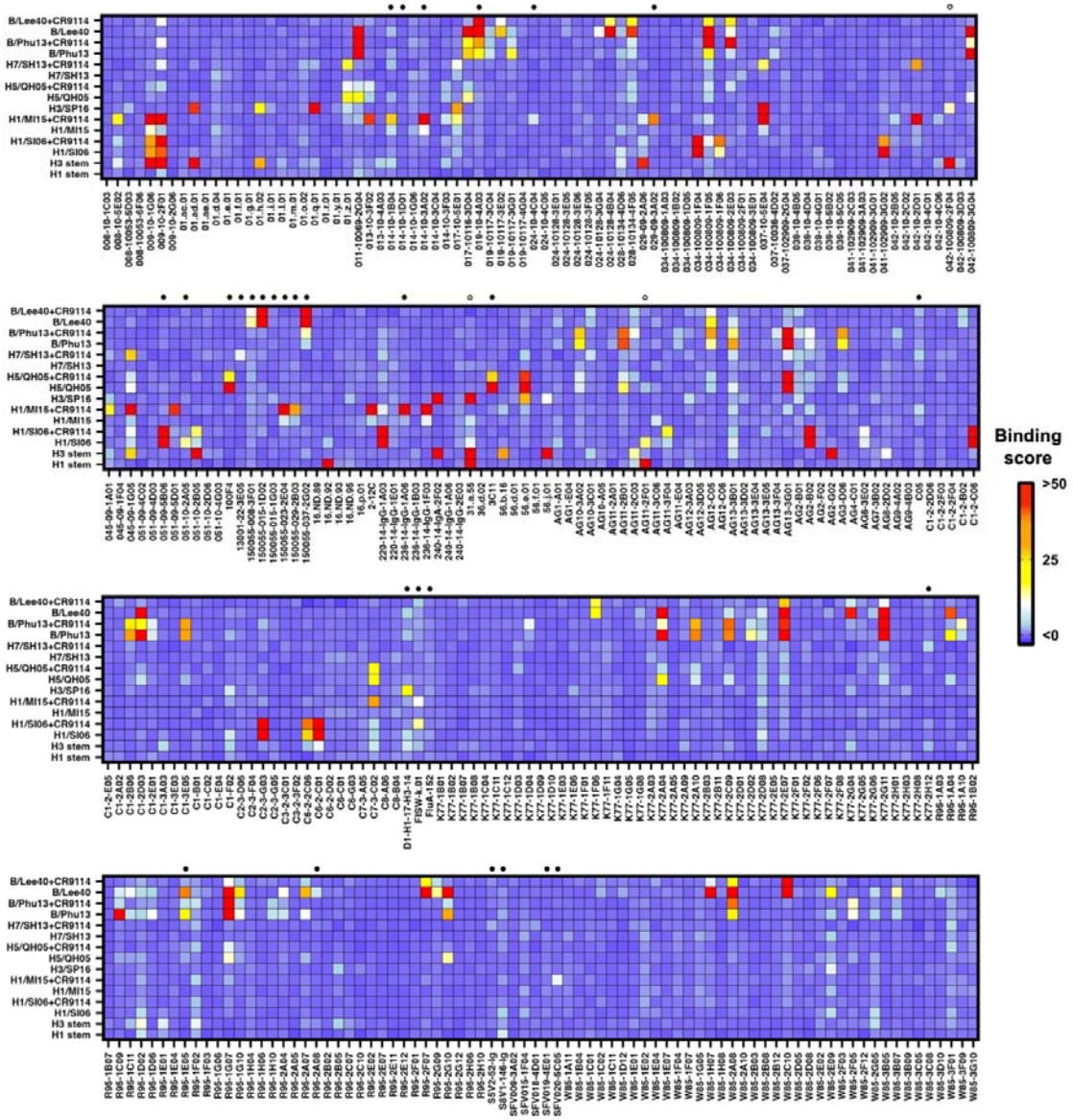

Figure 2. Rapid specificity characterization of the natively paired antibodies by mRNA display. The screening results of each scFv are shown as a heatmap. *X*-axis represents the scFv names. *Y*-axis represents each individual screens. Screens against CR9114 IgG pre-bound HAs are indicated by "+CR9114". Binding scores shown were adjusted with robust scaling. Individual cutoffs were set for each screen to determine positive hits (**Table S4, Materials and Methods**). Black circles at the top of the heatmap indicate head antibody controls, whereas empty circles indicate stem antibody controls.

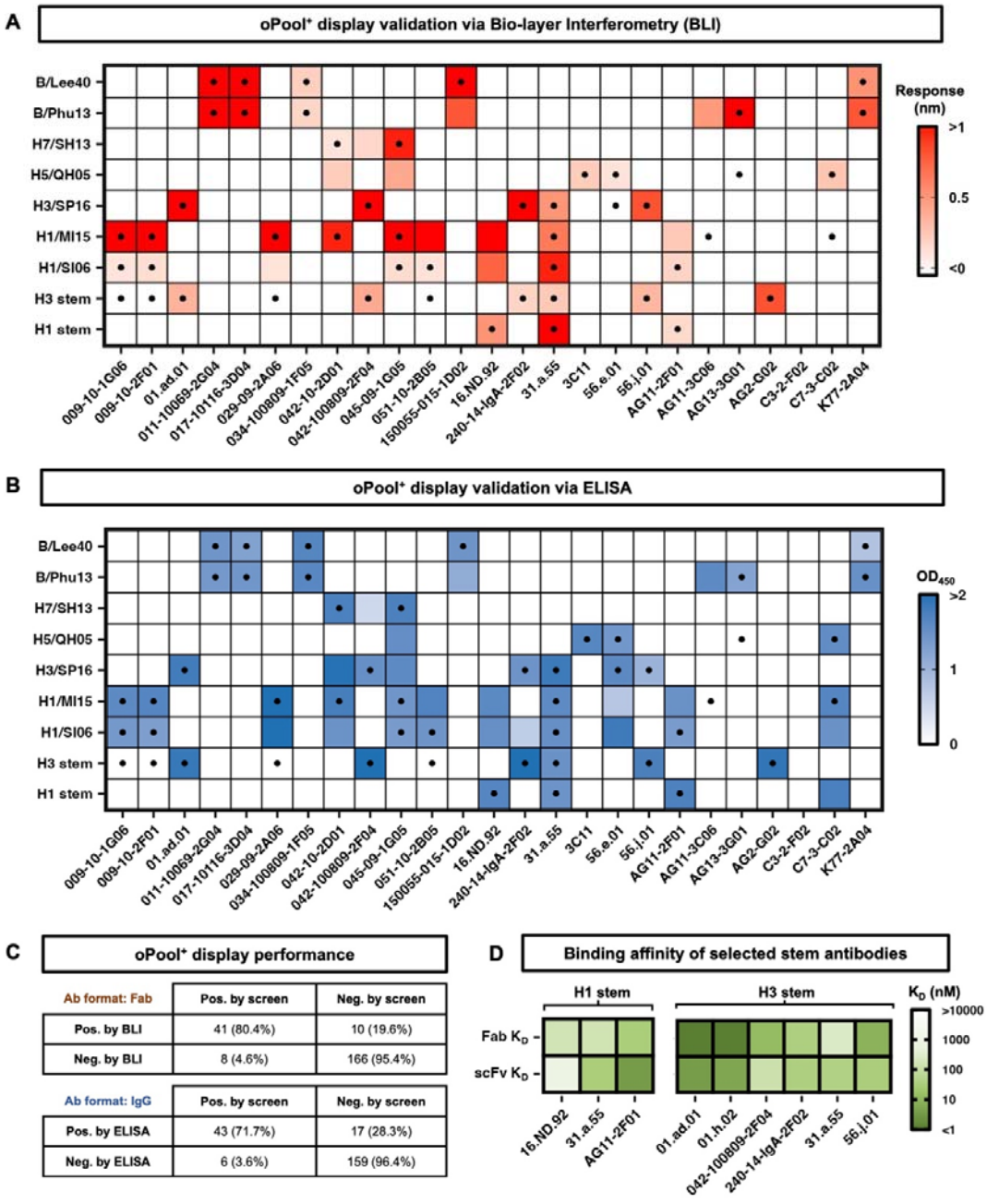

Figure 3. Systematic validation of oPool$^+$ display. (A-B) Binding activity of 25 antibodies against different HAs was measured by **(A)** biolayer interferometry (BLI) with antibodies in Fab format and **(B)** ELISA with antibodies in IgG format. **(A)** The response signals during the association phase and **(B)** the OD_{450} values were shown as heatmaps. The dots represent the hits in oPool$^+$ display. X-axis represents antibody names. Y-axis represents antigen names. **(C)** Binary confusion matrices based on BLI and ELISA validations are shown. **(D)**

831 Binding affinity of selected HA stem antibody candidates in both scFv and Fab format. Their
832 dissociation constants (K_D) against H1 stem and H3 stem are shown as heatmaps. Of note,
833 31.a.55 was a positive control for binding to both H1 stem and H3 stem[7], AG11-2F01 was a
834 positive control for binding to H1 stem[17], and 042-100809-2F04 was a positive control for
835 binding to H3 stem[54].

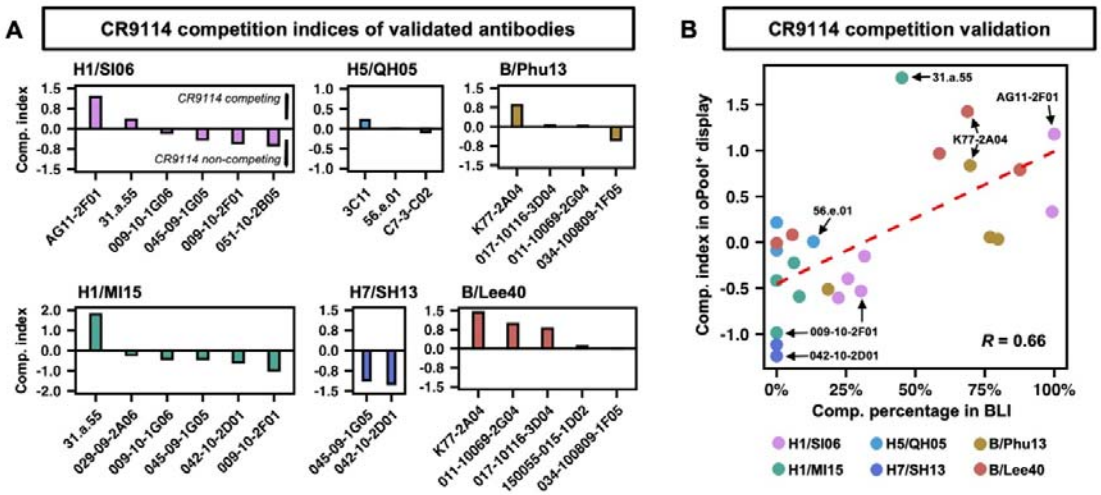

836

837 **Figure 4. CR9114 competition profile of validated antibodies. (A)** CR9114 competition
838 indices of validated antibodies. The competition indices calculated from oPool^{+} display are
839 shown. High positive values indicate CR9114 competition, low positive and high negative
840 values indicate no CR9114 competition. **(B)** CR9114 competition of validated antibodies
841 based on BLI results, shown as scatter plot against the competition indices. The response of
842 each antibody binding to the antigen were measured during the association step with or
843 without prior saturation binding of CR9114. The percentage of competition is shown with the
844 range of 0% (no competition) to 100% (complete competition). Pearson correlation
845 coefficient (*R*) between replicates is indicated. The linear fit lines are shown as red dash
846 lines. Representative antibodies are labelled.

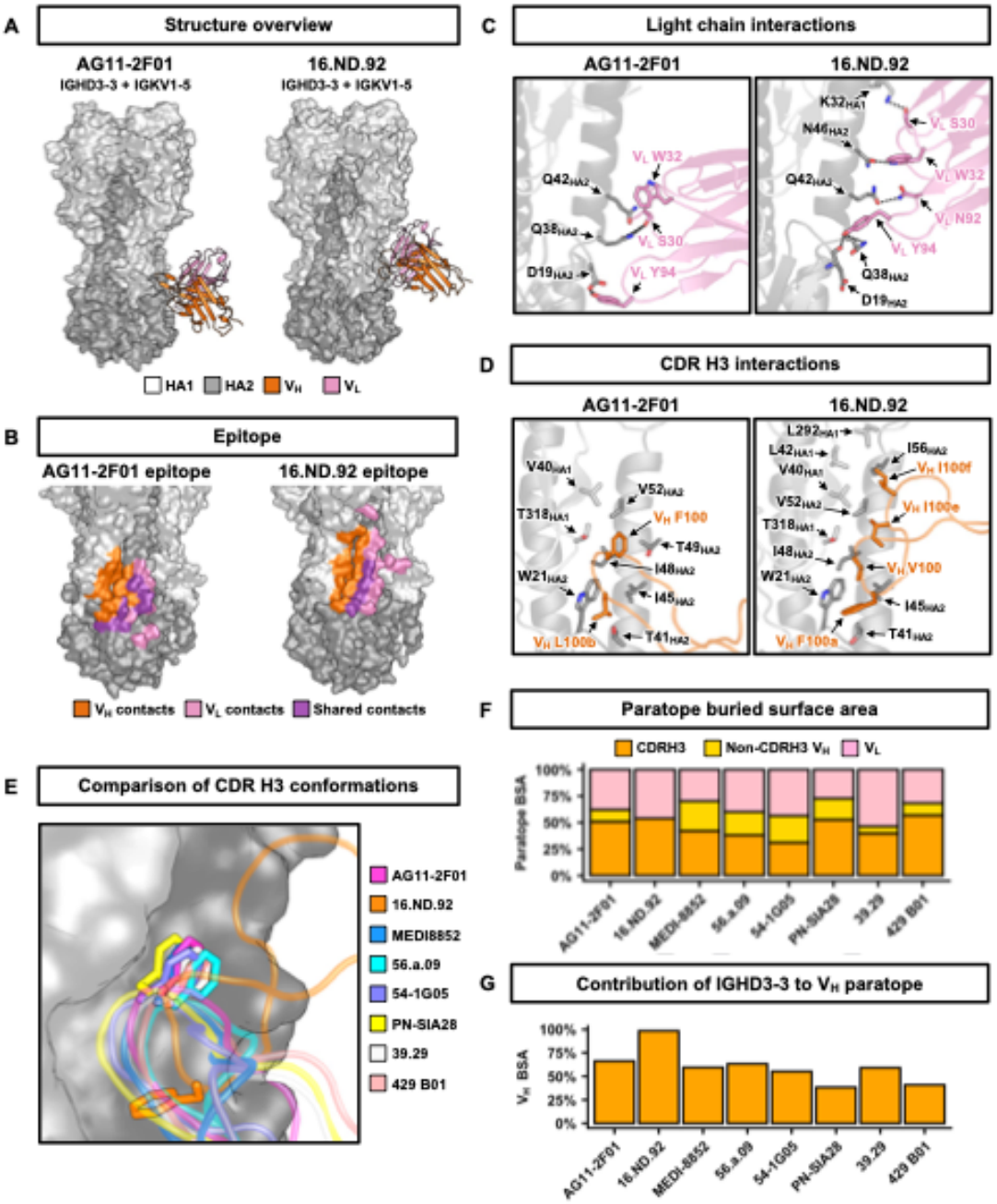

847

848 **Figure 5. Structural analysis of AG11-2F01 and 16.ND.92. (A)** Cryo-EM structures of
849 AG11-2F01 and 16.ND.92 in complex with H1/SI06 HA. HA1 is in light grey. HA2 is in dark
850 grey. Heavy chain variable domain (V_H) is in orange. Light chain variable domain (V_L) is in
851 pink. **(B)** Epitopes of AG11-2F01 and 16.ND.92. V_H contacts are in orange. V_L contacts are
852 in pink. Contacts shared by both V_H and V_L are in purple. **(C)** Interactions between light
853 chain and HA are shown. H-bonds are represented by black dashed lines. **(D)** Interactions

854 between CDR H3 and HA are shown. **(E)** Overlay of the CDR H3 loops from IGHD3-3 HA-
855 stem antibodies. HA is in surface representation. **(F)** Contributions of CDR H3 (orange), non-
856 CDR H3 V_H (yellow), and V_L (pink) to the paratope buried surface areas (BSA) of the
857 indicated antibodies. **(G)** Contributions of IGHD3-3-encoded residues to V_H paratope BSA of
858 the indicated antibodies.

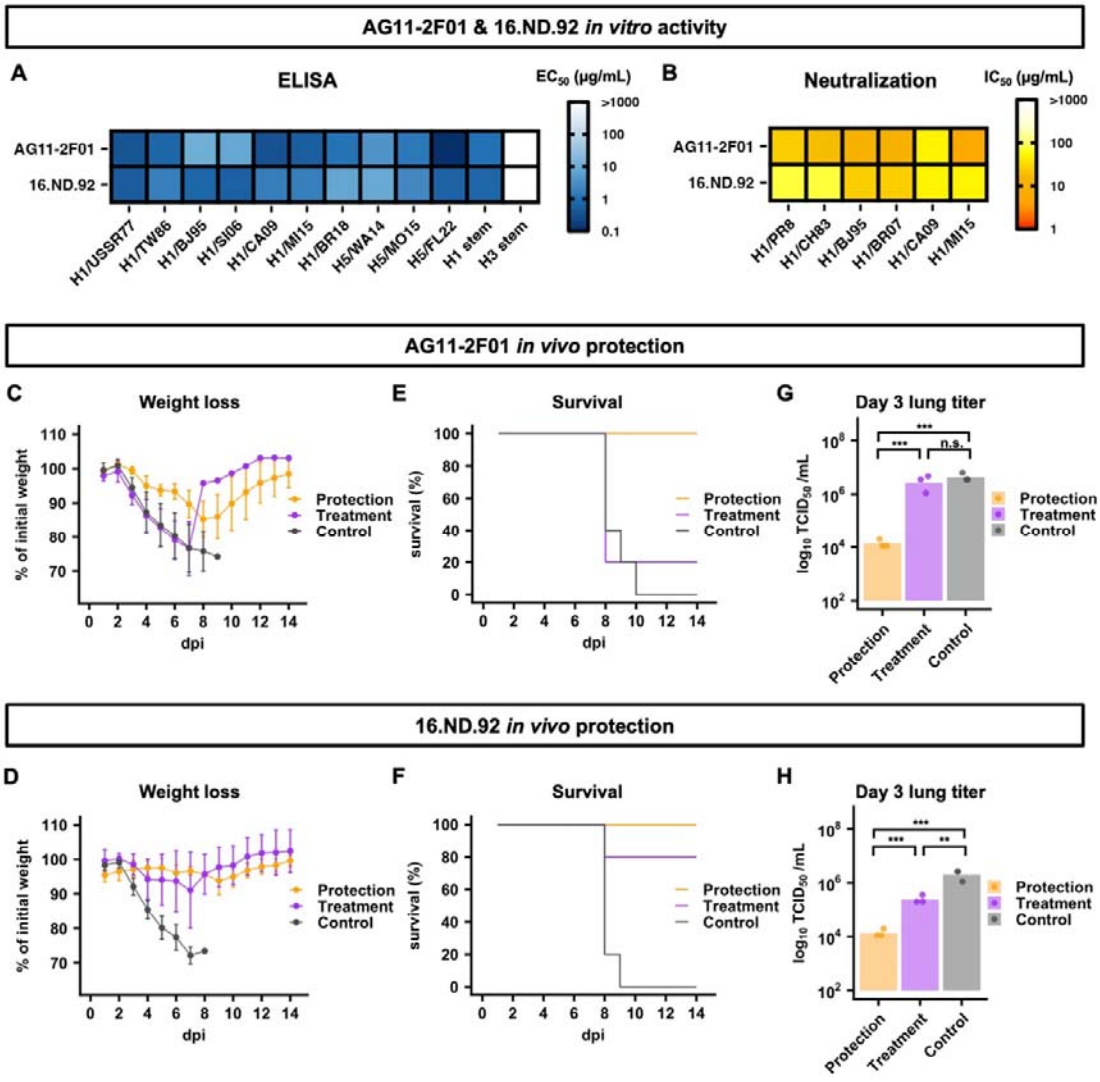

Figure 6. *in vitro* and *in vivo* protection of AG11-2F01 and 16.ND.92. (A) The binding activities of AG11-2F01 and 16.ND.92 against recombinant HA proteins from the indicated H1 and H5 strains were measured by ELISA. The EC_{50} values are shown as a heatmap. **(B)** The neutralization activity of AG11-2F01 and 16.ND.92 against different recombinant H1N1 viruses was measured by a microneutralization assay. The IC_{50} values are shown as a heatmap. **(A-B)** Strain names are abbreviated as follows: H1N1 A/Puerto Rico/8/1934 (H1/PR8), H1N1 A/USSR/90/1977 (H1/USSR77), H1N1 A/Chile/1/1983 (H1/CH83), H1N1 A/Taiwan/01/1986 (H1/TW86), H1N1 A/Beijing/262/1995 (H1/BJ95), H1N1 A/Solomon Island/3/2006 (H1/SI06), H1N1 A/Brisbane/59/2007 (H1/BR07), H1N1 A/California/04/2009 (H1/CA09), H1N1 A/Michigan/45/2015 (H1/MI15), H1N1 A/Brisbane/02/2018 (H1/BR18),

H5N8 A/northern pintail/WA/40964/2014 (H5/WA14), H5N2 A/snow goose/Missouri/CC15-84A/2015 (H5/MO15), and H5N1 A/bald eagle/Florida/W22-134-OP/2022 (H5/FL22). H1 stem and H3 stem represents the HA stem constructs designed based on H1N1 A/Brisbane/59/2007 HA and H3N2 A/Finland/486/2004 HA, respectively[29,30]. **(C-H)** The *in vivo* protection activity of AG11-2F01 and 16.ND.92 against lethal challenge of PR8 virus was assessed by **(C-D)** weight loss profiles, **(E-F)** Kaplan-Meier survival curves, and **(G-H)** lung viral titers at day 3 post-infection. *P* values were computed by two-tailed student's t-test. ***: $P < 0.001$; **: $P < 0.01$; n.s.: not significant.

SUPPLEMENTAL FIGURES

SUPPLEMENTAL TABLES

907 Table S10. Custom cutoff for each screen.

REFERENCES

1. Pedrioli, A., and Oxenius, A. (2021). Single B cell technologies for monoclonal antibody discovery. Trends Immunol. *42*, 1143–1158. https://doi.org/10.1016/j.it.2021.10.008.

2. Valldorf, B., Hinz, S.C., Russo, G., Pekar, L., Mohr, L., Klemm, J., Doerner, A., Krah, S., Hust, M., and Zielonka, S. (2022). Antibody display technologies: selecting the cream of the crop. Biol. Chem. *403*, 455–477. https://doi.org/10.1515/hsz-2020-0377.

3. Persson, M.A., Caothien, R.H., and Burton, D.R. (1991). Generation of diverse high-affinity human monoclonal antibodies by repertoire cloning. Proc. Natl. Acad. Sci. U. S. A. *88*, 2432–2436. https://doi.org/10.1073/pnas.88.6.2432.

4. Sheets, M.D., Amersdorfer, P., Finnern, R., Sargent, P., Lindquist, E., Schier, R., Hemingsen, G., Wong, C., Gerhart, J.C., and Marks, J.D. (1998). Efficient construction of a large nonimmune phage antibody library: the production of high-affinity human single-chain antibodies to protein antigens. Proc. Natl. Acad. Sci. U. S. A. *95*, 6157–6162. https://doi.org/10.1073/pnas.95.11.6157.

5. Kirkpatrick, E., Qiu, X., Wilson, P.C., Bahl, J., and Krammer, F. (2018). The influenza virus hemagglutinin head evolves faster than the stalk domain. Sci. Rep. *8*, 10432. https://doi.org/10.1038/s41598-018-28706-1.

6. Zost, S.J., Wu, N.C., Hensley, S.E., and Wilson, I.A. (2019). Immunodominance and antigenic variation of Influenza virus hemagglutinin: implications for design of universal vaccine immunogens. J. Infect. Dis. *219*, S38–S45. https://doi.org/10.1093/infdis/jiy696.

7. Joyce, M.G., Wheatley, A.K., Thomas, P.V., Chuang, G.-Y., Soto, C., Bailer, R.T., Druz, A., Georgiev, I.S., Gillespie, R.A., Kanekiyo, M., et al. (2016). Vaccine-induced antibodies that neutralize group 1 and group 2 influenza A viruses. Cell *166*, 609–623. https://doi.org/10.1016/j.cell.2016.06.043.

8. Corti, D., Voss, J., Gamblin, S.J., Codoni, G., Macagno, A., Jarrossay, D., Vachieri, S.G., Pinna, D., Minola, A., Vanzetta, F., et al. (2011). A neutralizing antibody selected from plasma cells that binds to group 1 and group 2 influenza A hemagglutinins. Science *333*, 850–856. https://doi.org/10.1126/science.1205669.

9. Kallewaard, N.L., Corti, D., Collins, P.J., Neu, U., McAuliffe, J.M., Benjamin, E., Wachter-Rosati, L., Palmer-Hill, F.J., Yuan, A.Q., Walker, P.A., et al. (2016). Structure and function analysis of an antibody aecognizing all influenza A subtypes. Cell *166*, 596–608. https://doi.org/10.1016/j.cell.2016.05.073.

10. Dreyfus, C., Laursen, N.S., Kwaks, T., Zuijdgeest, D., Khayat, R., Ekiert, D.C., Lee, J.H., Metlagel, Z., Bujny, M.V., Jongeneelen, M., et al. (2012). Highly conserved protective epitopes on influenza B viruses. Science *337*, 1343–1348. https://doi.org/10.1126/science.1222908.

11. Wu, N.C., and Wilson, I.A. (2020). Influenza hemagglutinin structures and antibody recognition. Cold Spring Harb. Perspect. Med. *10*, a038778. https://doi.org/10.1101/cshperspect.a038778.

12. Andrews, S.F., Graham, B.S., Mascola, J.R., and McDermott, A.B. (2018). Is it possible to develop a “universal” influenza virus vaccine? Immunogenetic considerations underlying B-cell biology in the development of a pan-subtype influenza A vaccine targeting the hemagglutinin stem. Cold Spring Harb. Perspect. Biol. *10*, a029413. https://doi.org/10.1101/cshperspect.a029413.

13. Pappas, L., Foglierini, M., Piccoli, L., Kallewaard, N.L., Turrini, F., Silacci, C., Fernandez-Rodriguez, B., Agatic, G., Giacchetto-Sasselli, I., Pellicciotta, G., et al. (2014). Rapid development of broadly influenza neutralizing antibodies through redundant mutations. Nature *516*, 418–422. https://doi.org/10.1038/nature13764.

14. Wu, N.C., Yamayoshi, S., Ito, M., Uraki, R., Kawaoka, Y., and Wilson, I.A. (2018). Recurring and adaptable binding motifs in broadly neutralizing antibodies to influenza virus are encoded on the D3-9 segment of the Ig gene. Cell Host Microbe *24*, 569-578.e4. https://doi.org/10.1016/j.chom.2018.09.010.

15. Cheung, C.S.-F., Fruehwirth, A., Paparoditis, P.C.G., Shen, C.-H., Foglierini, M., Joyce, M.G., Leung, K., Piccoli, L., Rawi, R., Silacci-Fregni, C., et al. (2020). Identification and structure of a multidonor class of head-directed influenza-neutralizing antibodies reveal the mechanism for its recurrent elicitation. Cell Rep. *32*, 108088. https://doi.org/10.1016/j.celrep.2020.108088.

16. Wang, Y., Lv, H., Teo, Q.W., Lei, R., Gopal, A.B., Ouyang, W.O., Yeung, Y.-H., Tan, T.J.C., Choi, D., Shen, I.R., et al. (2024). An explainable language model for antibody specificity prediction using curated influenza hemagglutinin antibodies. Immunity. https://doi.org/10.1016/j.immuni.2024.07.022.

17. Henry, C., Zheng, N.-Y., Huang, M., Cabanov, A., Rojas, K.T., Kaur, K., Andrews, S.F., Palm, A.-K.E., Chen, Y.-Q., Li, Y., et al. (2019). Influenza virus vaccination elicits poorly adapted B cell responses in elderly individuals. Cell Host Microbe *25*, 357-366.e6. https://doi.org/10.1016/j.chom.2019.01.002.

18. Andrews, S.F., Huang, Y., Kaur, K., Popova, L.I., Ho, I.Y., Pauli, N.T., Henry Dunand, C.J., Taylor, W.M., Lim, S., Huang, M., et al. (2015). Immune history profoundly affects broadly protective B cell responses to influenza. Sci. Transl. Med. *7*, 316ra192. https://doi.org/10.1126/scitranslmed.aad0522.

19. Dugan, H.L., Guthmiller, J.J., Arevalo, P., Huang, M., Chen, Y.-Q., Neu, K.E., Henry, C., Zheng, N.-Y., Lan, L.Y.-L., Tepora, M.E., et al. (2020). Preexisting immunity shapes distinct antibody landscapes after influenza virus infection and vaccination in humans. Sci. Transl. Med. *12*, eabd3601. https://doi.org/10.1126/scitranslmed.abd3601.

20. Ekiert, D.C., Kashyap, A.K., Steel, J., Rubrum, A., Bhabha, G., Khayat, R., Lee, J.H., Dillon, M.A., O'Neil, R.E., Faynboym, A.M., et al. (2012). Cross-neutralization of influenza A viruses mediated by a single antibody loop. Nature *489*, 526–532. https://doi.org/10.1038/nature11414.

21. Henry, C., Palm, A.-K.E., Utset, H.A., Huang, M., Ho, I.Y., Zheng, N.-Y., Fitzgerald, T., Neu, K.E., Chen, Y.-Q., Krammer, F., et al. (2019). Monoclonal antibody responses after recombinant hemagglutinin vaccine versus subunit inactivated influenza virus vaccine: a comparative study. J. Virol. *93*, e01150-19. https://doi.org/10.1128/JVI.01150-19.

22. Hu, H., Voss, J., Zhang, G., Buchy, P., Zuo, T., Wang, L., Wang, F., Zhou, F., Wang, G., Tsai, C., et al. (2012). A human antibody recognizing a conserved epitope of H5 hemagglutinin broadly neutralizes highly pathogenic avian influenza H5N1 viruses. J. Virol. *86*, 2978–2989. https://doi.org/10.1128/JVI.06665-11.

23. Liu, Y., Tan, H.-X., Koutsakos, M., Jegaskanda, S., Esterbauer, R., Tilmanis, D., Aban, M.,

994 Kedzierska, K., Hurt, A.C., Kent, S.J., et al. (2019). Cross-lineage protection by human
995 antibodies binding the influenza B hemagglutinin. Nat. Commun. *10*, 324.
996 https://doi.org/10.1038/s41467-018-08165-y.

997 24. Watanabe, A., McCarthy, K.R., Kuraoka, M., Schmidt, A.G., Adachi, Y., Onodera, T.,
998 Tonouchi, K., Caradonna, T.M., Bajic, G., Song, S., et al. (2019). Antibodies to a
999 conserved Influenza head interface epitope protect by an IgG subtype-dependent
1000 mechanism. Cell *177*, 1124-1135.e16. https://doi.org/10.1016/j.cell.2019.03.048.

1001 25. Lee, J., Boutz, D.R., Chromikova, V., Joyce, M.G., Vollmers, C., Leung, K., Horton, A.P.,
1002 DeKosky, B.J., Lee, C.-H., Lavinder, J.J., et al. (2016). Molecular-level analysis of the
1003 serum antibody repertoire in young adults before and after seasonal influenza
1004 vaccination. Nat. Med. *22*, 1456–1464. https://doi.org/10.1038/nm.4224.

1005 26. Roberts, R.W., and Szostak, J.W. (1997). RNA-peptide fusions for the in vitro selection
1006 of peptides and proteins. Proc. Natl. Acad. Sci. U. S. A. *94*, 12297–12302.
1007 https://doi.org/10.1073/pnas.94.23.12297.

1008 27. Wu, N.C., Dai, L., Olson, C.A., Lloyd-Smith, J.O., and Sun, R. (2016). Adaptation in
1009 protein fitness landscapes is facilitated by indirect paths. eLife *5*, e16965.
1010 https://doi.org/10.7554/eLife.16965.

1011 28. Tanaka, S., Olson, C.A., Barnes, C.O., Higashide, W., Gonzalez, M., Taft, J., Richardson,
1012 A., Martin-Fernandez, M., Bogunovic, D., Gnanapragasam, P.N.P., et al. (2022). Rapid
1013 identification of neutralizing antibodies against SARS-CoV-2 variants by mRNA display.
1014 Cell Rep. *38*, 110348. https://doi.org/10.1016/j.celrep.2022.110348.

1015 29. Impagliazzo, A., Milder, F., Kuipers, H., Wagner, M.V., Zhu, X., Hoffman, R.M.B., van
1016 Meersbergen, R., Huizingh, J., Wanningen, P., Verspuij, J., et al. (2015). A stable trimeric
1017 influenza hemagglutinin stem as a broadly protective immunogen. Science *349*, 1301–
1018 1306. https://doi.org/10.1126/science.aac7263.

1019 30. Corbett, K.S., Moin, S.M., Yassine, H.M., Cagigi, A., Kanekiyo, M., Boyoglu-Barnum, S.,
1020 Myers, S.I., Tsybovsky, Y., Wheatley, A.K., Schramm, C.A., et al. (2019). Design of
1021 nanoparticulate group 2 influenza virus hemagglutinin stem antigens that activate
1022 unmutated ancestor B cell receptors of broadly neutralizing antibody lineages. mBio *10*,

e02810-18. https://doi.org/10.1128/mBio.02810-18.

31. Wu, N.C., Andrews, S.F., Raab, J.E., O'Connell, S., Schramm, C.A., Ding, X., Chambers, M.J., Leung, K., Wang, L., Zhang, Y., et al. (2020). Convergent evolution in breadth of two VH6-1-encoded Influenza antibody clonotypes from a single donor. Cell Host Microbe *28*, 434-444.e4. https://doi.org/10.1016/j.chom.2020.06.003.

32. Matsuda, K., Huang, J., Zhou, T., Sheng, Z., Kang, B.H., Ishida, E., Griesman, T., Stuccio, S., Bolkhovitinov, L., Wohlbold, T.J., et al. (2019). Prolonged evolution of the memory B cell response induced by a replicating adenovirus-influenza H5 vaccine. Sci. Immunol. *4*, eaau2710. https://doi.org/10.1126/sciimmunol.aau2710.

33. Chen, Y., Wang, F., Yin, L., Jiang, H., Lu, X., Bi, Y., Zhang, W., Shi, Y., Burioni, R., Tong, Z., et al. (2022). Structural basis for a human broadly neutralizing influenza A hemagglutinin stem-specific antibody including H17/18 subtypes. Nat. Commun. *13*, 7603. https://doi.org/10.1038/s41467-022-35236-y.

34. Nakamura, G., Chai, N., Park, S., Chiang, N., Lin, Z., Chiu, H., Fong, R., Yan, D., Kim, J., Zhang, J., et al. (2013). An in vivo human-plasmablast enrichment technique allows rapid identification of therapeutic influenza A antibodies. Cell Host Microbe *14*, 93–103. https://doi.org/10.1016/j.chom.2013.06.004.

35. Lanzavecchia, A., Frühwirth, A., Perez, L., and Corti, D. (2016). Antibody-guided vaccine design: identification of protective epitopes. Curr. Opin. Immunol. *41*, 62–67. https://doi.org/10.1016/j.coi.2016.06.001.

36. Haynes, B.F., Wiehe, K., Borrow, P., Saunders, K.O., Korber, B., Wagh, K., McMichael, A.J., Kelsoe, G., Hahn, B.H., Alt, F., et al. (2023). Strategies for HIV-1 vaccines that induce broadly neutralizing antibodies. Nat. Rev. Immunol. *23*, 142–158. https://doi.org/10.1038/s41577-022-00753-w.

37. Toussi, S.S., Hammond, J.L., Gerstenberger, B.S., and Anderson, A.S. (2023). Therapeutics for COVID-19. Nat. Microbiol. *8*, 771–786. https://doi.org/10.1038/s41564-023-01356-4.

38. Schoeder, C.T., Gilchuk, P., Sangha, A.K., Ledwitch, K.V., Malherbe, D.C., Zhang, X.,

Binshtein, E., Williamson, L.E., Martina, C.E., Dong, J., et al. (2022). Epitope-focused immunogen design based on the ebolavirus glycoprotein HR2-MPER region. PLOS Pathog. *18*, e1010518. https://doi.org/10.1371/journal.ppat.1010518.

39. Hunt, A.C., Vögeli, B., Hassan, A.O., Guerrero, L., Kightlinger, W., Yoesep, D.J., Krüger, A., DeWinter, M., Diamond, M.S., Karim, A.S., et al. (2023). A rapid cell-free expression and screening platform for antibody discovery. Nat. Commun. *14*, 3897. https://doi.org/10.1038/s41467-023-38965-w.

40. Liu, L., Iketani, S., Guo, Y., Reddem, E.R., Casner, R.G., Nair, M.S., Yu, J., Chan, J.F.-W., Wang, M., Cerutti, G., et al. (2022). An antibody class with a common CDRH3 motif broadly neutralizes sarbecoviruses. Sci. Transl. Med. *14*, eabn6859. https://doi.org/10.1126/scitranslmed.abn6859.

41. Liu, H., Kaku, C.I., Song, G., Yuan, M., Andrabi, R., Burton, D.R., Walker, L.M., and Wilson, I.A. (2022). Human antibodies to SARS-CoV-2 with a recurring YYDRxG motif retain binding and neutralization to variants of concern including Omicron. Commun. Biol. *5*, 766. https://doi.org/10.1038/s42003-022-03700-6.

42. Robinson, J.E., Hastie, K.M., Cross, R.W., Yenni, R.E., Elliott, D.H., Rouelle, J.A., Kannadka, C.B., Smira, A.A., Garry, C.E., Bradley, B.T., et al. (2016). Most neutralizing human monoclonal antibodies target novel epitopes requiring both Lassa virus glycoprotein subunits. Nat. Commun. *7*, 11544. https://doi.org/10.1038/ncomms11544.

43. Chen, L., Sun, M., Zhang, H., Zhang, X., Yao, Y., Li, M., Li, K., Fan, P., Zhang, H., Qin, Y., et al. (2024). Potent human neutralizing antibodies against Nipah virus derived from two ancestral antibody heavy chains. Nat. Commun. *15*, 2987. https://doi.org/10.1038/s41467-024-47213-8.

44. Joubbi, S., Micheli, A., Milazzo, P., Maccari, G., Ciano, G., Cardamone, D., and Medini, D. (2024). Antibody design using deep learning: from sequence and structure design to affinity maturation. Brief. Bioinform. *25*, bbae307. https://doi.org/10.1093/bib/bbae307.

45. Bennett, N.R., Watson, J.L., Ragotte, R.J., Borst, A.J., See, D.L., Weidle, C., Biswas, R., Shrock, E.L., Leung, P.J.Y., Huang, B., et al. (2024). Atomically accurate de novo design of single-domain antibodies. BioRxiv Prepr. Serv. Biol., 2024.03.14.585103.

https://doi.org/10.1101/2024.03.14.585103.

46. Frey, N.C., Hotzel, I., Stanton, S.D., Kelly, R.L., Alberstein, R.G., Makowski, E.K., Martinkus, K., Berenberg, D., Bevers, J., Bryson, T., et al. (2025). Lab-in-the-loop therapeutic antibody design with deep learning. Preprint at bioRxiv, https://doi.org/10.1101/2025.02.19.639050 https://doi.org/10.1101/2025.02.19.639050.

47. Wu, N.C., Grande, G., Turner, H.L., Ward, A.B., Xie, J., Lerner, R.A., and Wilson, I.A. (2017). In vitro evolution of an influenza broadly neutralizing antibody is modulated by hemagglutinin receptor specificity. Nat. Commun. *8*, 15371. https://doi.org/10.1038/ncomms15371.

48. Quintero-Hernández, V., Juárez-González, V.R., Ortíz-León, M., Sánchez, R., Possani, L.D., and Becerril, B. (2007). The change of the scFv into the Fab format improves the stability and in vivo toxin neutralization capacity of recombinant antibodies. Mol. Immunol. *44*, 1307–1315. https://doi.org/10.1016/j.molimm.2006.05.009.

49. Kang, T.H., and Seong, B.L. (2020). Solubility, stability, and avidity of recombinant antibody fragments expressed in microorganisms. Front. Microbiol. *11*. https://doi.org/10.3389/fmicb.2020.01927.

50. Rondot, S., Koch, J., Breitling, F., and Dübel, S. (2001). A helper phage to improve single-chain antibody presentation in phage display. Nat. Biotechnol. *19*, 75–78. https://doi.org/10.1038/83567.

51. Chao, G., Lau, W.L., Hackel, B.J., Sazinsky, S.L., Lippow, S.M., and Wittrup, K.D. (2006). Isolating and engineering human antibodies using yeast surface display. Nat. Protoc. *1*, 755–768. https://doi.org/10.1038/nprot.2006.94.

52. Huang, K.-Y.A., Rijal, P., Schimanski, L., Powell, T.J., Lin, T.-Y., McCauley, J.W., Daniels, R.S., and Townsend, A.R. (2015). Focused antibody response to influenza linked to antigenic drift. J. Clin. Invest. *125*, 2631–2645. https://doi.org/10.1172/JCI81104.

53. Li, G.-M., Chiu, C., Wrammert, J., McCausland, M., Andrews, S.F., Zheng, N.-Y., Lee, J.-H., Huang, M., Qu, X., Edupuganti, S., et al. (2012). Pandemic H1N1 influenza vaccine induces a recall response in humans that favors broadly cross-reactive memory B cells.

Proc. Natl. Acad. Sci. U. S. A. *109*, 9047–9052. https://doi.org/10.1073/pnas.1118979109.

54. Henry Dunand, C.J., Leon, P.E., Kaur, K., Tan, G.S., Zheng, N.-Y., Andrews, S., Huang, M., Qu, X., Huang, Y., Salgado-Ferrer, M., et al. (2015). Preexisting human antibodies neutralize recently emerged H7N9 influenza strains. J. Clin. Invest. *125*, 1255–1268. https://doi.org/10.1172/JCI74374.

55. Swindells, M.B., Porter, C.T., Couch, M., Hurst, J., Abhinandan, K.R., Nielsen, J.H., Macindoe, G., Hetherington, J., and Martin, A.C.R. (2017). abYsis: Integrated antibody sequence and structure-management, analysis, and prediction. J. Mol. Biol. *429*, 356–364. https://doi.org/10.1016/j.jmb.2016.08.019.

56. Fu, L., Niu, B., Zhu, Z., Wu, S., and Li, W. (2012). CD-HIT: accelerated for clustering the next-generation sequencing data. Bioinformatics *28*, 3150–3152. https://doi.org/10.1093/bioinformatics/bts565.

57. Camacho, C., Coulouris, G., Avagyan, V., Ma, N., Papadopoulos, J., Bealer, K., and Madden, T.L. (2009). BLAST+: architecture and applications. BMC Bioinformatics *10*, 421. https://doi.org/10.1186/1471-2105-10-421.

58. Olson, C.A., Wu, N.C., and Sun, R. (2014). A comprehensive biophysical description of pairwise epistasis throughout an entire protein domain. Curr. Biol. *24*, 2643–2651. https://doi.org/10.1016/j.cub.2014.09.072.

59. Cock, P.J.A., Antao, T., Chang, J.T., Chapman, B.A., Cox, C.J., Dalke, A., Friedberg, I., Hamelryck, T., Kauff, F., Wilczynski, B., et al. (2009). Biopython: freely available Python tools for computational molecular biology and bioinformatics. Bioinformatics *25*, 1422–1423. https://doi.org/10.1093/bioinformatics/btp163.

60. Punjani, A., Rubinstein, J.L., Fleet, D.J., and Brubaker, M.A. (2017). cryoSPARC: algorithms for rapid unsupervised cryo-EM structure determination. Nat. Methods *14*, 290–296. https://doi.org/10.1038/nmeth.4169.

61. Leem, J., Dunbar, J., Georges, G., Shi, J., and Deane, C.M. (2016). ABodyBuilder: automated antibody structure prediction with data–driven accuracy estimation. mAbs *8*, 1259–1268. https://doi.org/10.1080/19420862.2016.1205773.

62. Laursen, N.S., Friesen, R.H.E., Zhu, X., Jongeneelen, M., Blokland, S., Vermond, J., van Eijgen, A., Tang, C., van Diepen, H., Obmolova, G., et al. (2018). Universal protection against influenza infection by a multidomain antibody to influenza hemagglutinin. Science *362*, 598–602. https://doi.org/10.1126/science.aaq0620.

63. Pettersen, E.F., Goddard, T.D., Huang, C.C., Couch, G.S., Greenblatt, D.M., Meng, E.C., and Ferrin, T.E. (2004). UCSF Chimera--a visualization system for exploratory research and analysis. J. Comput. Chem. *25*, 1605–1612. https://doi.org/10.1002/jcc.20084.

64. Emsley, P., and Cowtan, K. (2004). Coot: model-building tools for molecular graphics. Acta Crystallogr. D Biol. Crystallogr. *60*, 2126–2132. https://doi.org/10.1107/S0907444904019158.

65. Afonine, P.V., Poon, B.K., Read, R.J., Sobolev, O.V., Terwilliger, T.C., Urzhumtsev, A., and Adams, P.D. (2018). Real-space refinement in PHENIX for cryo-EM and crystallography. Acta Crystallogr. Sect. Struct. Biol. *74*, 531–544. https://doi.org/10.1107/S2059798318006551.

66. Benton, D.J., Nans, A., Calder, L.J., Turner, J., Neu, U., Lin, Y.P., Ketelaars, E., Kallewaard, N.L., Corti, D., Lanzavecchia, A., et al. (2018). Influenza hemagglutinin membrane anchor. Proc. Natl. Acad. Sci. U. S. A. *115*, 10112–10117. https://doi.org/10.1073/pnas.1810927115.

67. Sanchez-Garcia, R., Gomez-Blanco, J., Cuervo, A., Carazo, J.M., Sorzano, C.O.S., and Vargas, J. (2021). DeepEMhancer: a deep learning solution for cryo-EM volume post-processing. Commun. Biol. *4*, 874. https://doi.org/10.1038/s42003-021-02399-1.

68. Ruffolo, J.A., Chu, L.-S., Mahajan, S.P., and Gray, J.J. (2023). Fast, accurate antibody structure prediction from deep learning on massive set of natural antibodies. Nat. Commun. *14*, 2389. https://doi.org/10.1038/s41467-023-38063-x.

69. Millán, C., McCoy, A.J., Terwilliger, T.C., and Read, R.J. (2023). Likelihood-based docking of models into cryo-EM maps. Acta Crystallogr. Sect. Struct. Biol. *79*, 281–289. https://doi.org/10.1107/S2059798323001602.

70. Krissinel, E., and Henrick, K. (2007). Inference of macromolecular assemblies from

1164 crystalline state. J. Mol. Biol. *372*, 774–797. https://doi.org/10.1016/j.jmb.2007.05.022.

1165 71. Ye, J., Ma, N., Madden, T.L., and Ostell, J.M. (2013). IgBLAST: an immunoglobulin
1166 variable domain sequence analysis tool. Nucleic Acids Res. *41*, W34-40.
1167 https://doi.org/10.1093/nar/gkt382.

1168 72. Neumann, G., Fujii, K., Kino, Y., and Kawaoka, Y. (2005). An improved reverse genetics
1169 system for influenza A virus generation and its implications for vaccine production. Proc.
1170 Natl. Acad. Sci. U. S. A. *102*, 16825–16829. https://doi.org/10.1073/pnas.0505587102.

1171 73. Lei, R., Kim, W., Lv, H., Mou, Z., Scherm, M.J., Schmitz, A.J., Turner, J.S., Tan, T.J.C.,
1172 Wang, Y., Ouyang, W.O., et al. (2023). Leveraging vaccination-induced protective
1173 antibodies to define conserved epitopes on influenza N2 neuraminidase. Immunity *56*,
1174 2621-2634.e6. https://doi.org/10.1016/j.immuni.2023.10.005.

1175 74. Overdijk, M.B., Verploegen, S., Ortiz Buijsse, A., Vink, T., Leusen, J.H.W., Bleeker, W.K.,
1176 and Parren, P.W.H.I. (2012). Crosstalk between human IgG isotypes and murine effector
1177 cells. J. Immunol. Baltim. Md 1950 *189*, 3430–3438.
1178 https://doi.org/10.4049/jimmunol.1200356.

1179 75. Dekkers, G., Bentlage, A.E.H., Stegmann, T.C., Howie, H.L., Lissenberg-Thunnissen, S.,
1180 Zimring, J., Rispens, T., and Vidarsson, G. (2017). Affinity of human IgG subclasses to
1181 mouse Fc gamma receptors. mAbs *9*, 767–773.
1182 https://doi.org/10.1080/19420862.2017.1323159.

1183

A Library breakdown

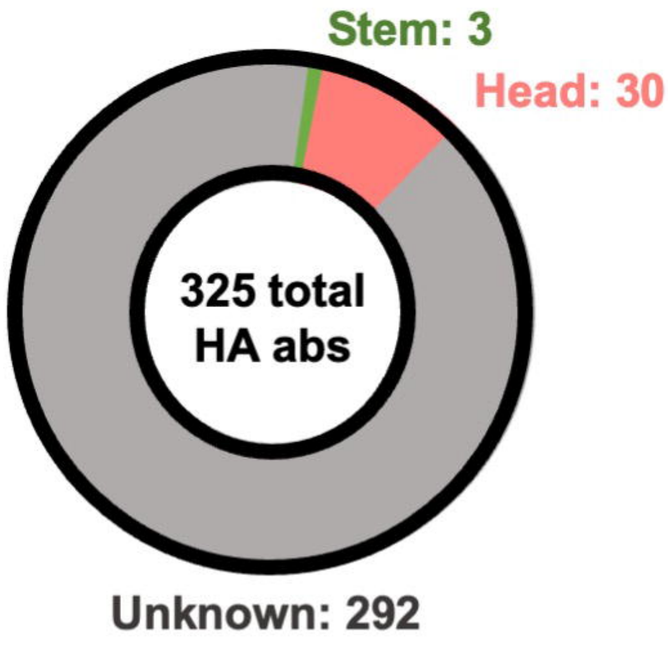

B scFv construct design

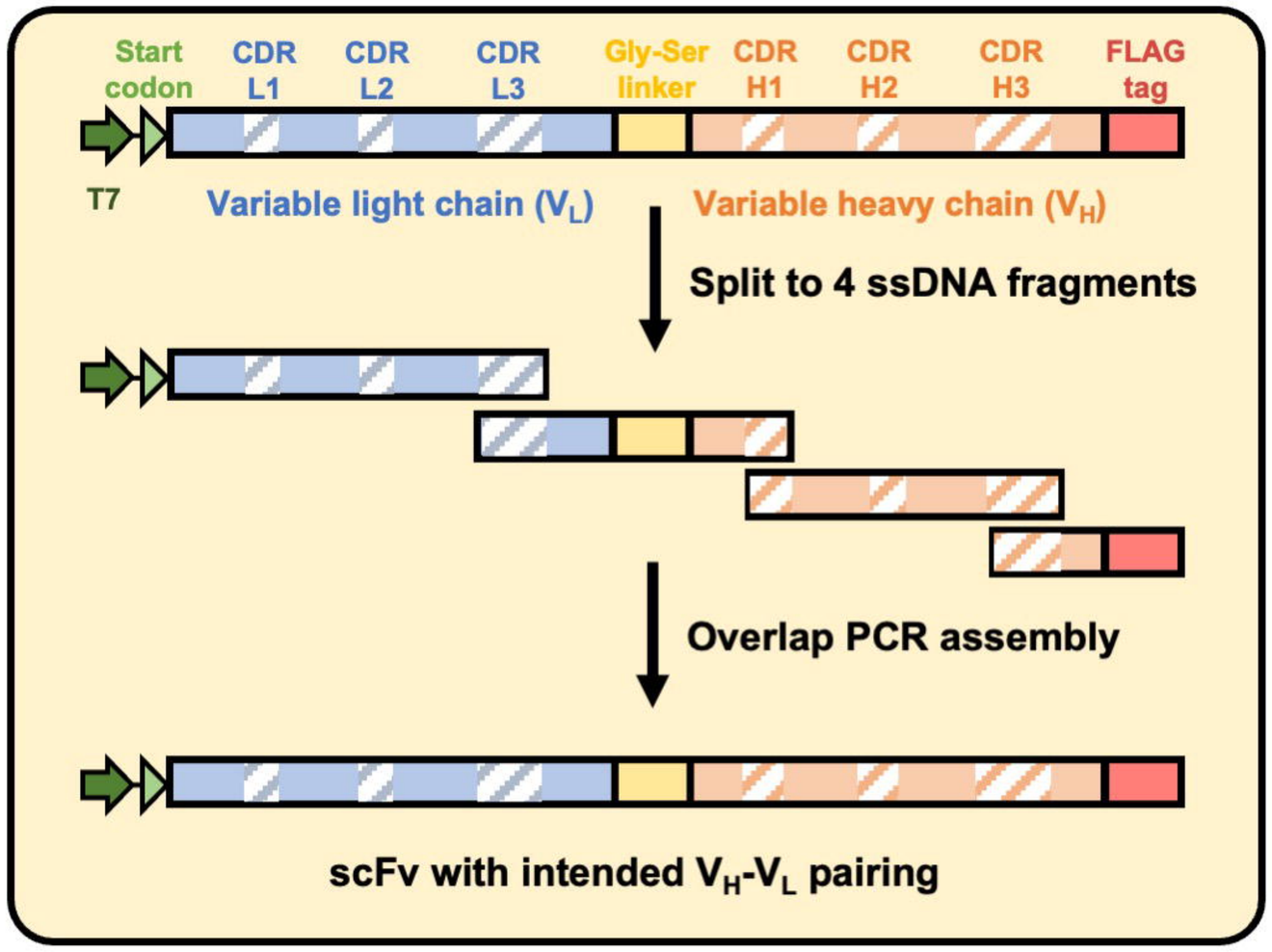

C Parallel assembly of natively paired scFvs

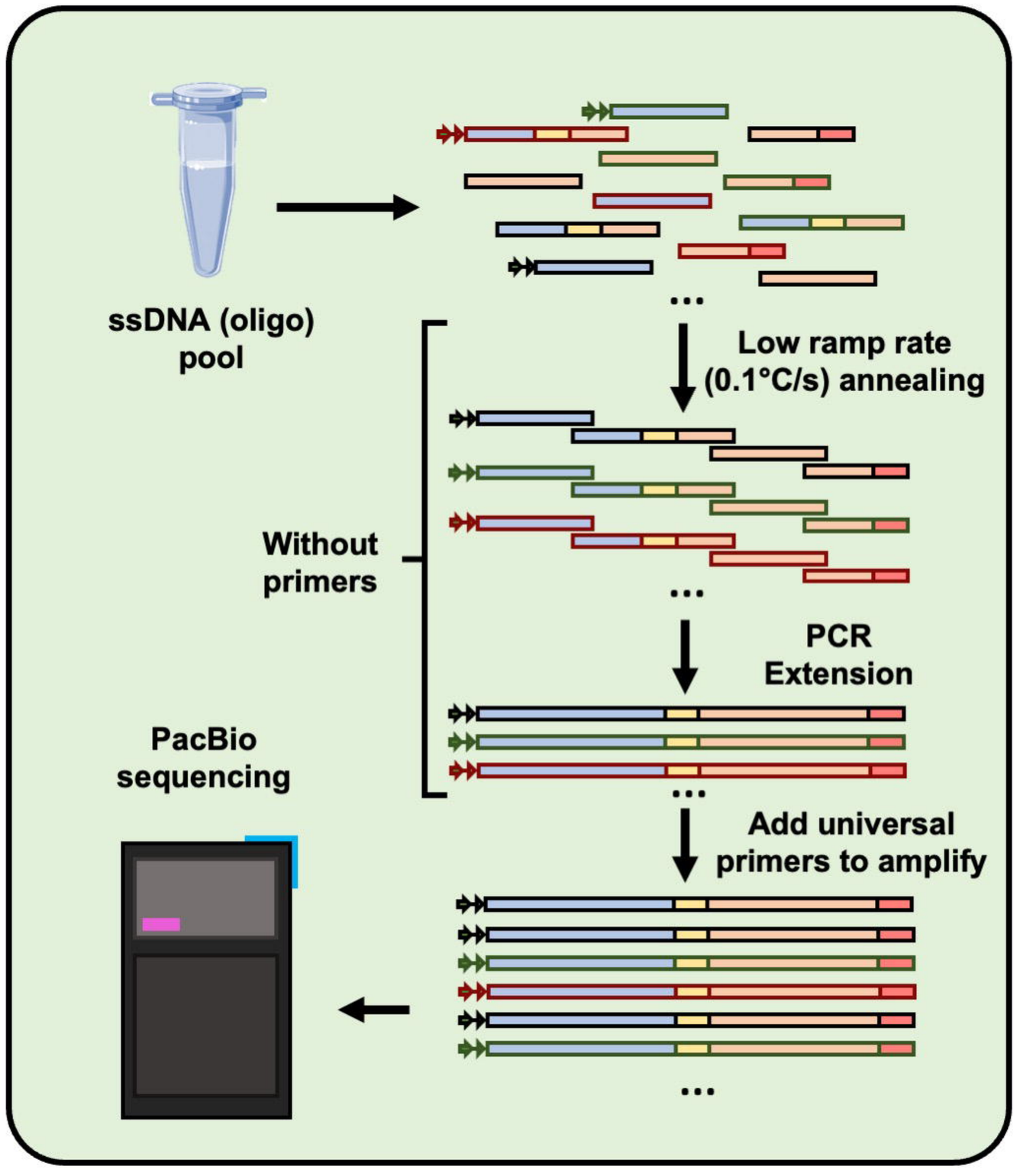

D Assembled product

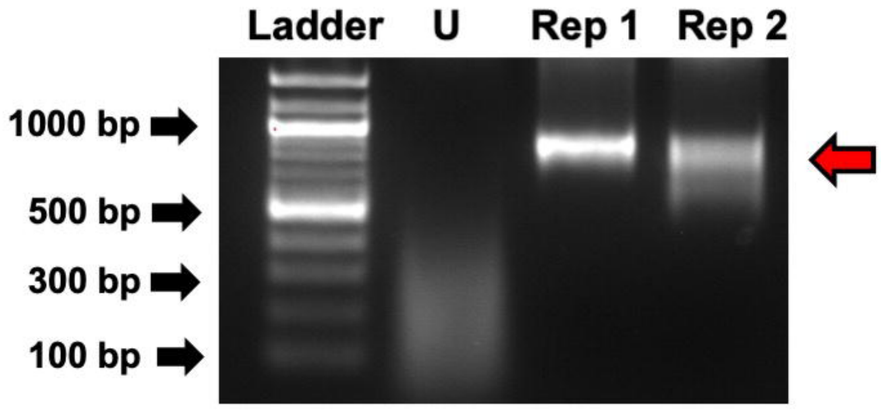

E One-pot PCR reproducibility

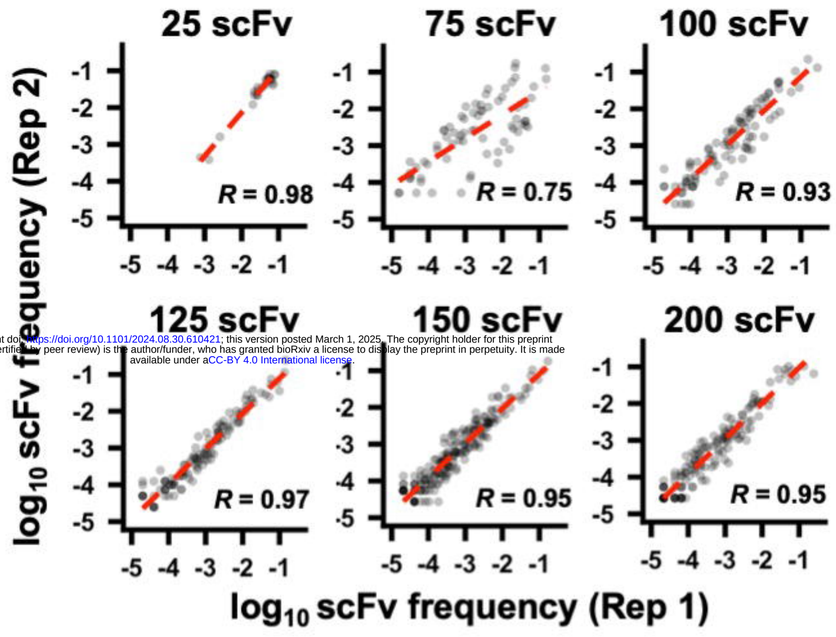

F One-pot PCR coverage

PCR size	Coverage
25 scFv	25/25 (100%)
75 scFv	73/75 (97.3%)
100 scFv	93/100 (93%)
125 scFv	115/125 (92%)
150 scFv	138/150 (92%)
200 scFv	180/200 (90%)

B/Lee40+CR9114
B/Lee40
B/Phu13+CR9114
B/Phu13
H7/SH13+CR9114
H7/SH13
H5/QH05+CR9114
H5/QH05
H3/SP16
H1/MI15+CR9114
H1/MI15
H1/SI06+CR9114
H1/SI06
H3 stem
H1 stem

008-10-1C03
008-10-5E02
008-10053-5D03
008-10053-6F06
009-10-1G06
009-10-2F01
009-10-2G06
01.ac.01
01.ad.01
01.ae.01
01.d.04
01.e.01
01.f.01
01.g.01
01.h.02
01.i.01
01.l.01
01.m.01
01.o.02
01.q.01
01.r.01
01.y.01
01.z.01
011-10069-2G04
013-10-3F02
013-10-4A03
014-10-1B04
014-10-1D01
014-10-1G06
014-10-3A02
014-10-3C04
014-10-3F03
017-10-5E01
017-10116-3D04
019-10-4A03
019-101117-3C04
019-101117-3E02
019-10117-3G01
019-10117-4G04
024-10-4C04
024-10-4C05
024-10128-3E01
024-10128-3E05
024-10128-3E06
024-10128-3F05
024-10128-3G04
024-10128-4B04
028-10134-4D06
028-10134-4F05
029-09-2A06
029-09-3A02
034-100809-1A03
034-100809-1B02
034-100809-1D05
034-100809-1F04
034-100809-1F05
034-100809-1F06
034-100809-2E03
034-100809-2F01
034-100809-3E01
037-10-5E04
037-10036-4D02
037-102909-2G04
039-10-4B05
039-10-4D04
039-10-4G01
039-10-5B02
039-10-5C05
041-102909-2C03
041-102909-3A03
041-102909-3G01
041-102909-3G02
042-10-2B05
042-10-2C02
042-10-2D01
042-10-4C01
042-10-4C06
042-100809-2F04
042-100809-3D03
042-100809-3G04

045-09-1A01
045-09-1F04
045-09-1G05
051-09-4C02
051-09-4D03
051-09-5B06
051-09-5D01
051-10-2A05
051-10-2B05
051-10-2D06
051-10-4G03
100F4
13001-22-3E05
150055-008-3F01
150055-015-1D02
150055-015-1G03
150055-023-2E04
150055-029-2B03
150055-037-2G02
16.ND.89
16.ND.92
16.ND.93
16.ND.95
16.p.01
2-12C
220-14-IgG-1A03
220-14-IgG-1E01
236-14-IgG-1A06
236-14-IgG-1B03
236-14-IgG-1F03
240-14-IgA-2F02
240-14-IgG-1A06
240-14-IgG-2E03
31.a.55
36.d.02
3C11
56.b.16
56.d.01
56.e.01
56.f.01
56.j.01
AG1-A01
AG1-E04
AG10-3A02
AG10-3C01
AG10-A05
AG11-2A01
AG11-2B01
AG11-2C03
AG11-2F01
AG11-3C06
AG11-3F04
AG11-E04
AG12-3A03
AG12-3D05
AG12-C05
AG12-C06
AG13-3B01
AG13-3D02
AG13-3E04
AG13-3E05
AG13-3F04
AG13-3G01
AG2-B01
AG2-B02
AG2-F02
AG2-G02
AG3-D06
AG4-C01
AG6-3E02
AG7-3B02
AG8-2D02
AG9-4A02
AG9-4B03
C05
C1-2-2D06
C1-2-2F03
C1-2-2F04
C1-2-B02
C1-2-C06

C1-2-E05
C1-2A02
C1-2B06
C1-2D03
C1-2E01
C1-3A03
C1-3E03
C1-3E05
C1-B01
C1-C02
C1-E04
C1-F02
C2-3-D06
C2-3-F04
C2-3-G03
C2-3-G05
C3-2-3C01
C3-2-3F02
C6-2-2C06
C6-2-C01
C6-2-D02
C6-C01
C6-G03
C7-3-A05
C7-3-C02
C8-A06
C8-B04
D1-H1-17-H3-14
FISW-k.01
FluA-152
K77-1B01
K77-1B02
K77-1B07
K77-1B08
K77-1C04
K77-1C11
K77-1C12
K77-1D03
K77-1D04
K77-1D09
K77-1D10
K77-1E03
K77-1E06
K77-1F01
K77-1F06
K77-1F11
K77-1G04
K77-1G05
K77-1G08
K77-2A03
K77-2A04
K77-2A05
K77-2A09
K77-2A10
K77-2B03
K77-2B11
K77-2C09
K77-2D01
K77-2D02
K77-2D08
K77-2E05
K77-2E07
K77-2F01
K77-2F02
K77-2F06
K77-2F07
K77-2F08
K77-2G04
K77-2G05
K77-2G06
K77-2G11
K77-2H01
K77-2H03
K77-2H08
K77-2H12
R95-1A03
R95-1A04
R95-1A10
R95-1B02

R95-1B07
R95-1C09
R95-1C11
R95-1D02
R95-1D06
R95-1E01
R95-1E04
R95-1E05
R95-1F02
R95-1F03
R95-1G06
R95-1G07
R95-1G10
R95-1H04
R95-1H06
R95-1H10
R95-2A04
R95-2A05
R95-2A07
R95-2A08
R95-2B02
R95-2B05
R95-2C07
R95-2C10
R95-2E02
R95-2E07
R95-2E11
R95-2E12
R95-2F01
R95-2F07
R95-2G09
R95-2G10
R95-2G12
R95-2H06
R95-2H10
S5V2-52-Ig
S8V1-146-Ig
SFV009-3A02
SFV015-1F04
SFV018-4D01
SFV019-4E01
SFV020-5C05
W85-1A11
W85-1B04
W85-1C01
W85-1C02
W85-1C11
W85-1D12
W85-1E01
W85-1E02
W85-1E04
W85-1E07
W85-1F04
W85-1F07
W85-1G05
W85-1H07
W85-1H08
W85-2A08
W85-2A10
W85-2B03
W85-2B08
W85-2B12
W85-2C10
W85-2D05
W85-2D08
W85-2E02
W85-2E09
W85-2F03
W85-2F05
W85-2F12
W85-2G05
W85-3B05
W85-3B07
W85-3B09
W85-3C05
W85-3C08
W85-3D10
W85-3F01
W85-3F09
W85-3G10

Binding score
>50
25
<0

A oPool+ display validation via Bio-layer Interferometry (BLI)

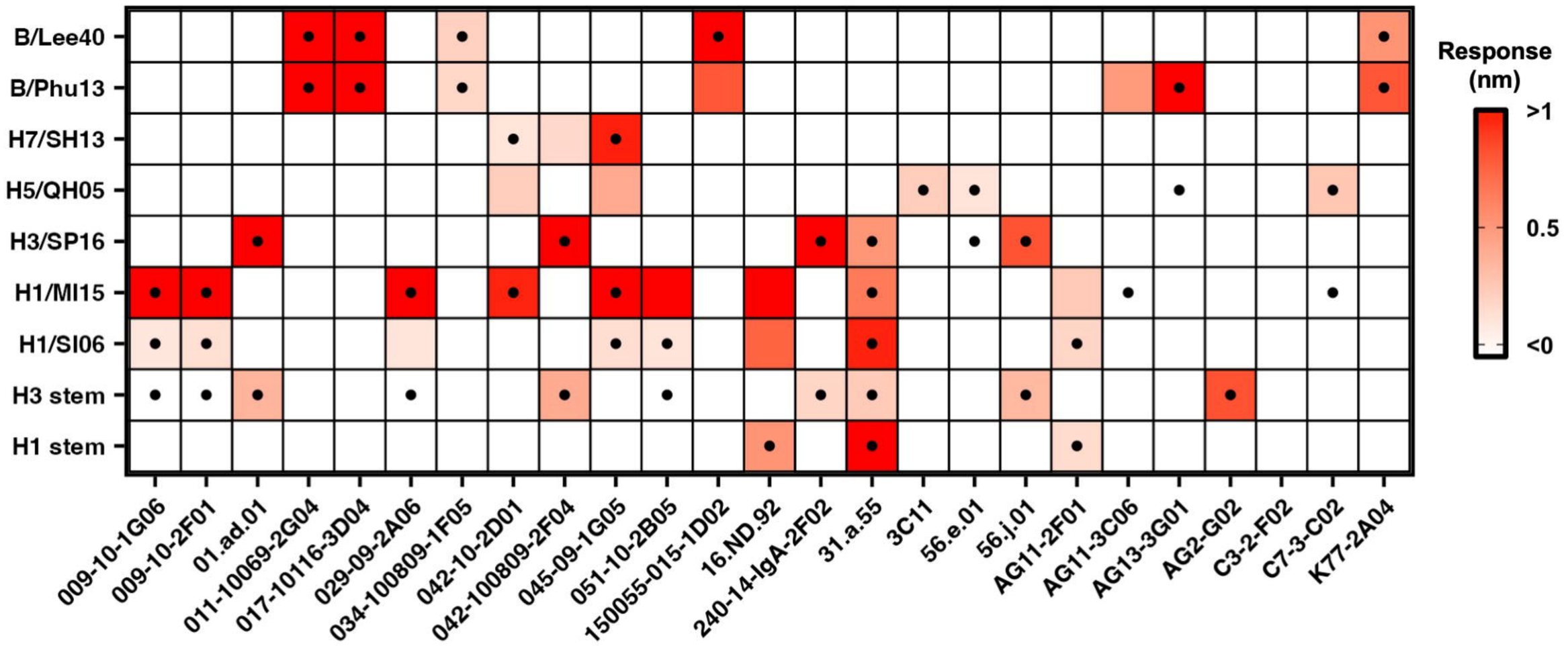

B oPool+ display validation via ELISA

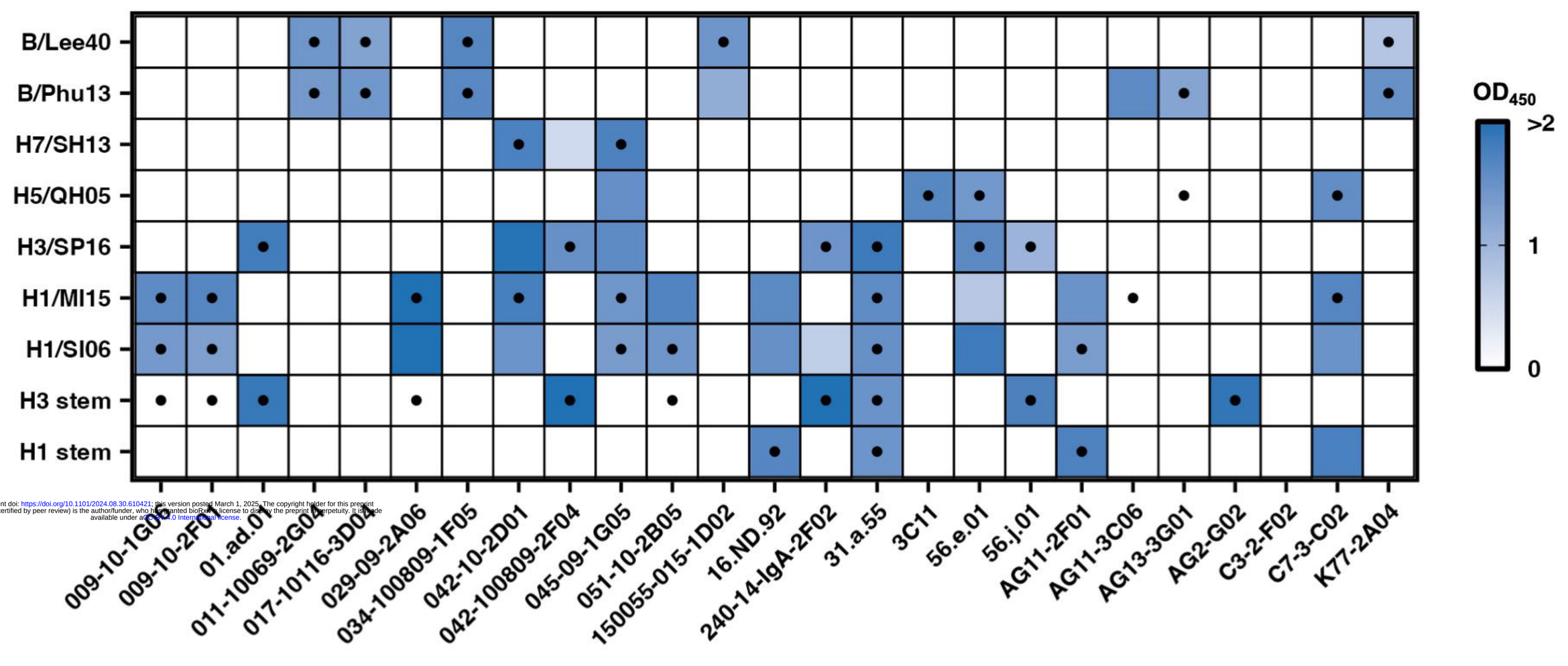

C oPool+ display performance

Ab format: Fab	Pos. by screen	Neg. by screen
Pos. by BLI	41 (80.4%)	10 (19.6%)
Neg. by BLI	8 (4.6%)	166 (95.4%)

Ab format: IgG	Pos. by screen	Neg. by screen
Pos. by ELISA	43 (71.7%)	17 (28.3%)
Neg. by ELISA	6 (3.6%)	159 (96.4%)

D Binding affinity of selected stem antibodies

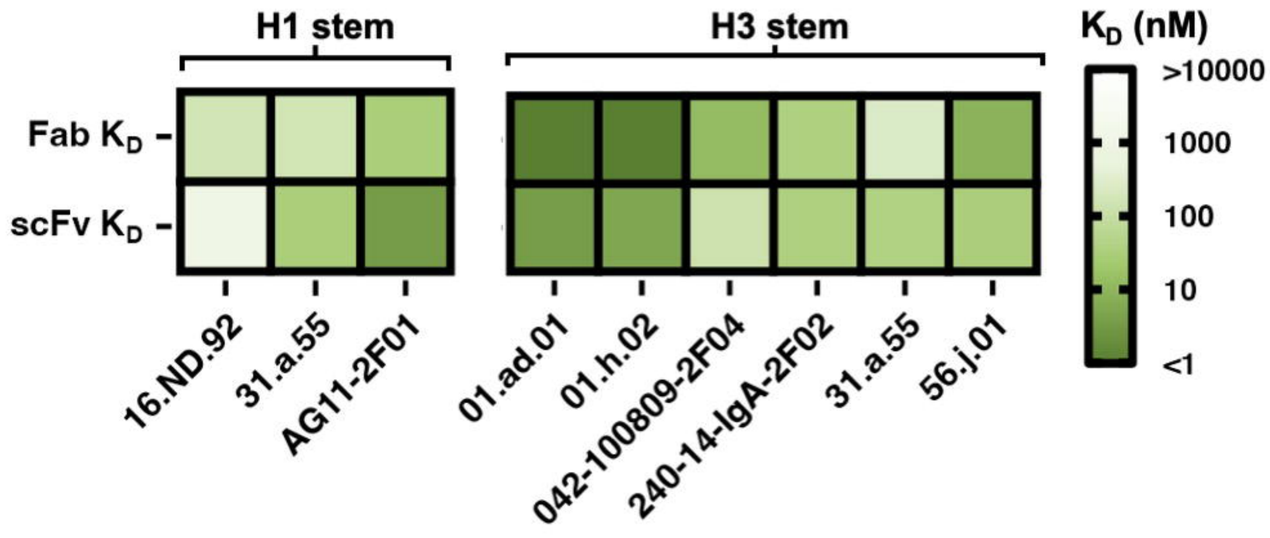

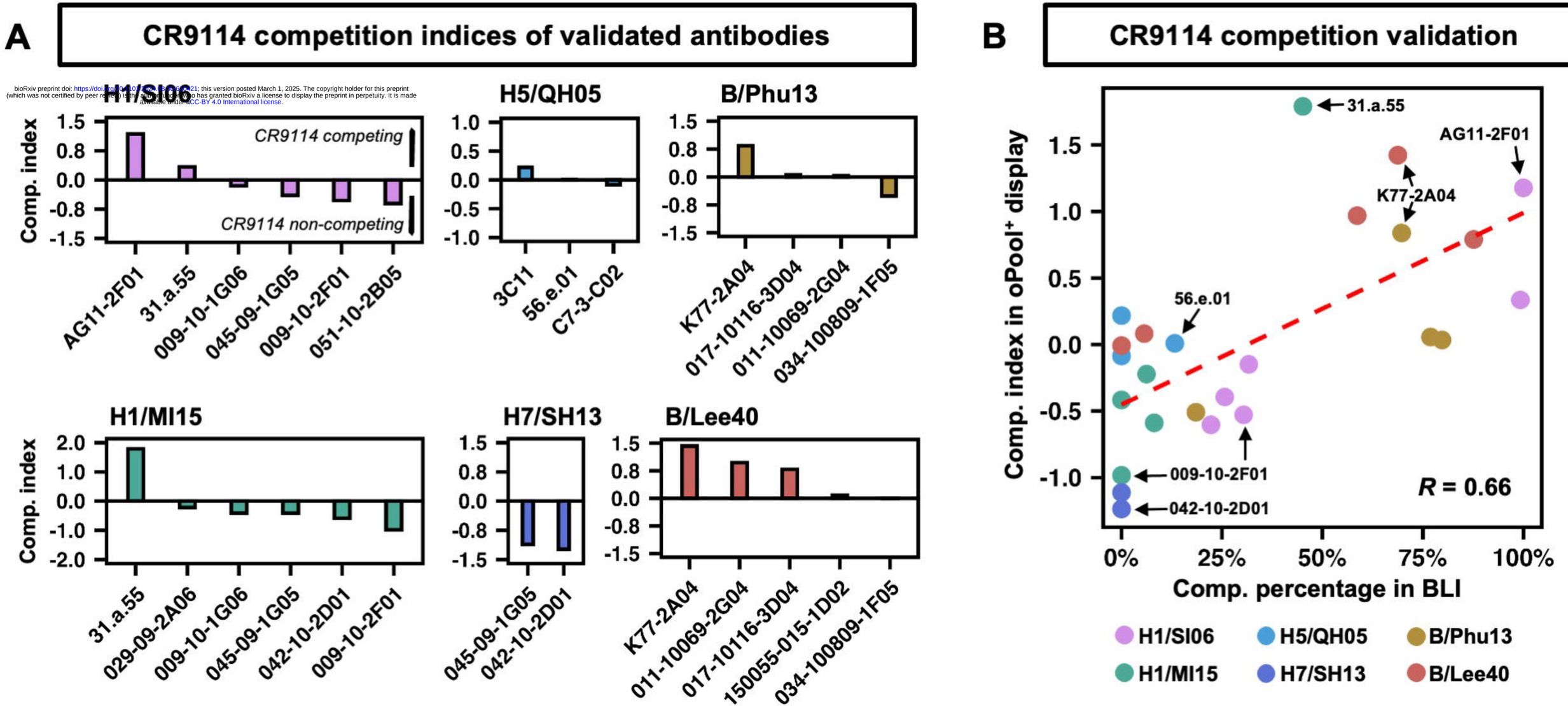

A

Structure overview

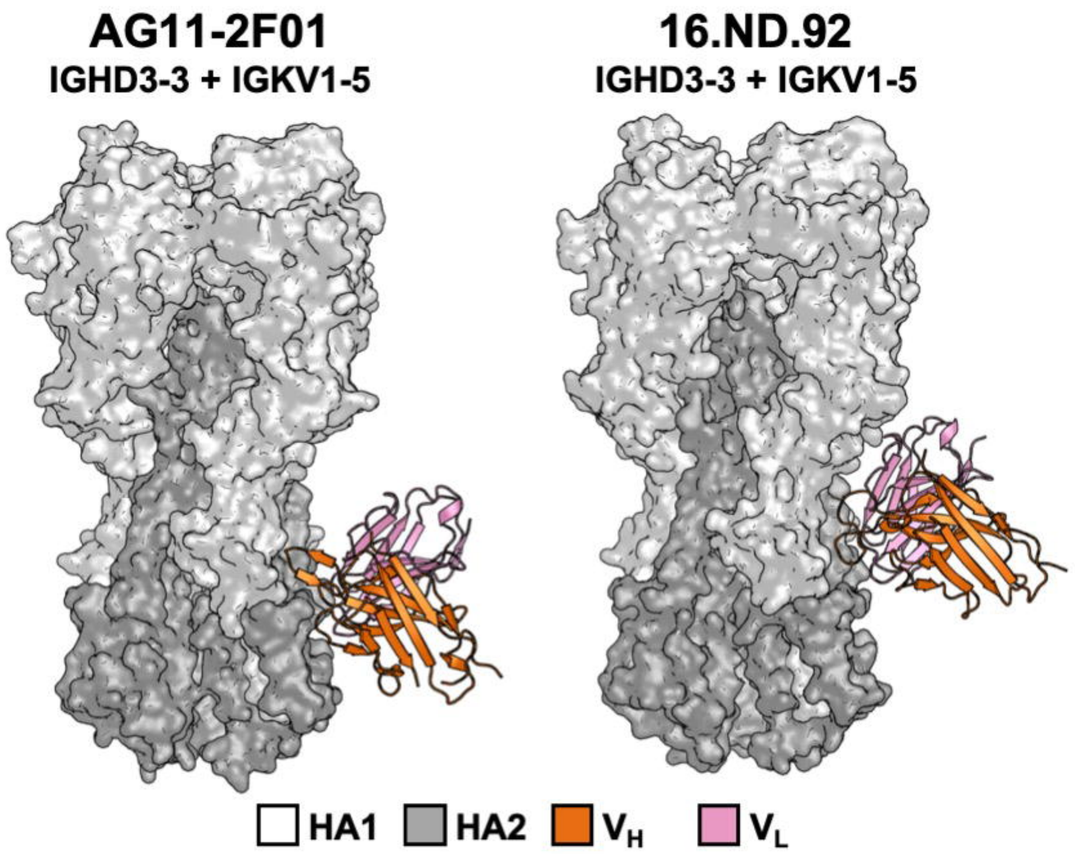

B

Epitope

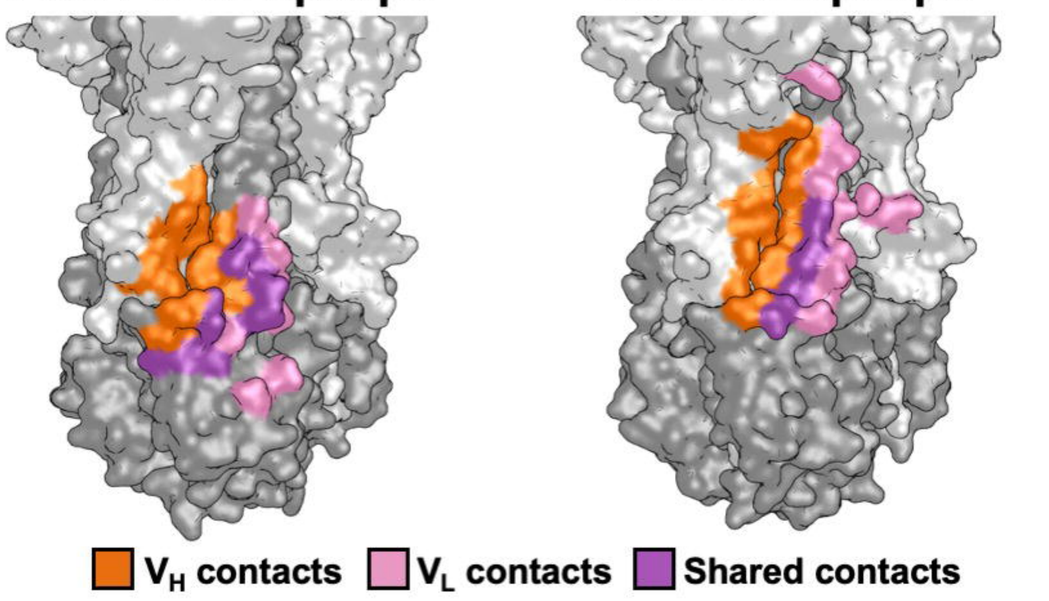

C

Light chain interactions

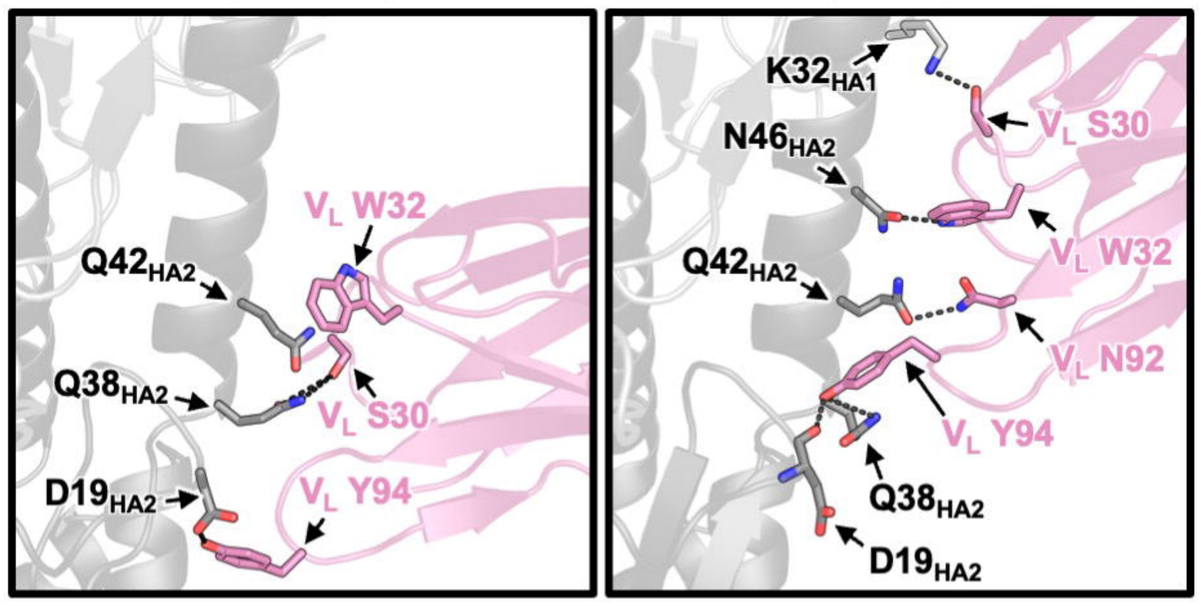

D

CDR H3 interactions

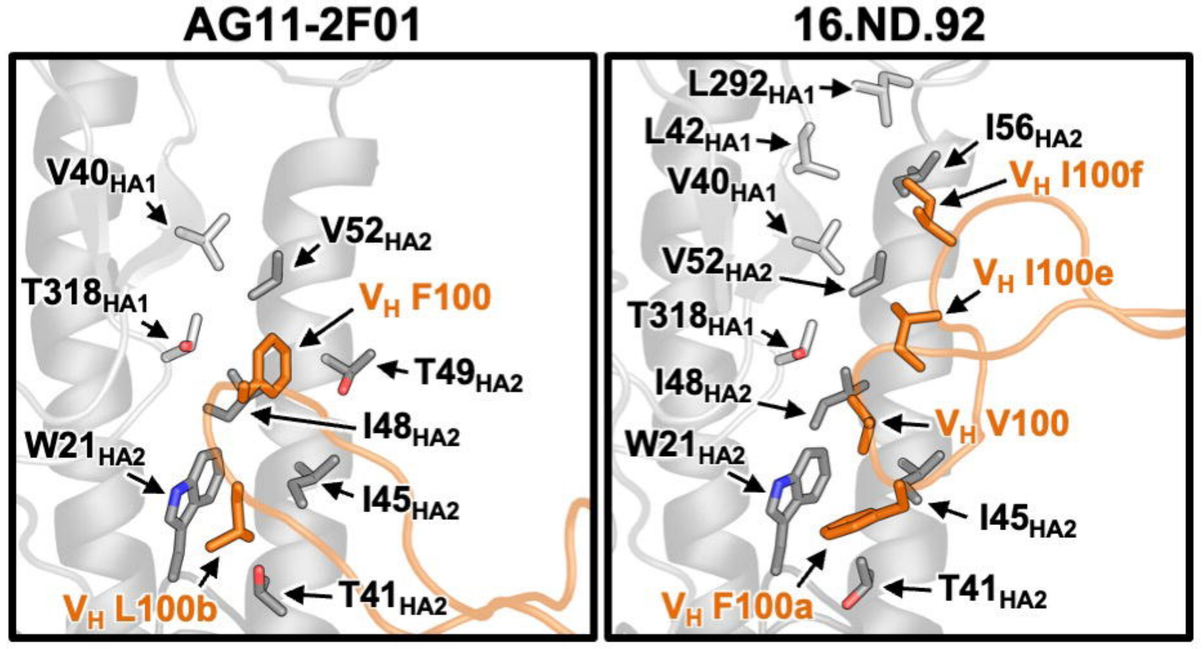

E

Comparison of CDR H3 conformations

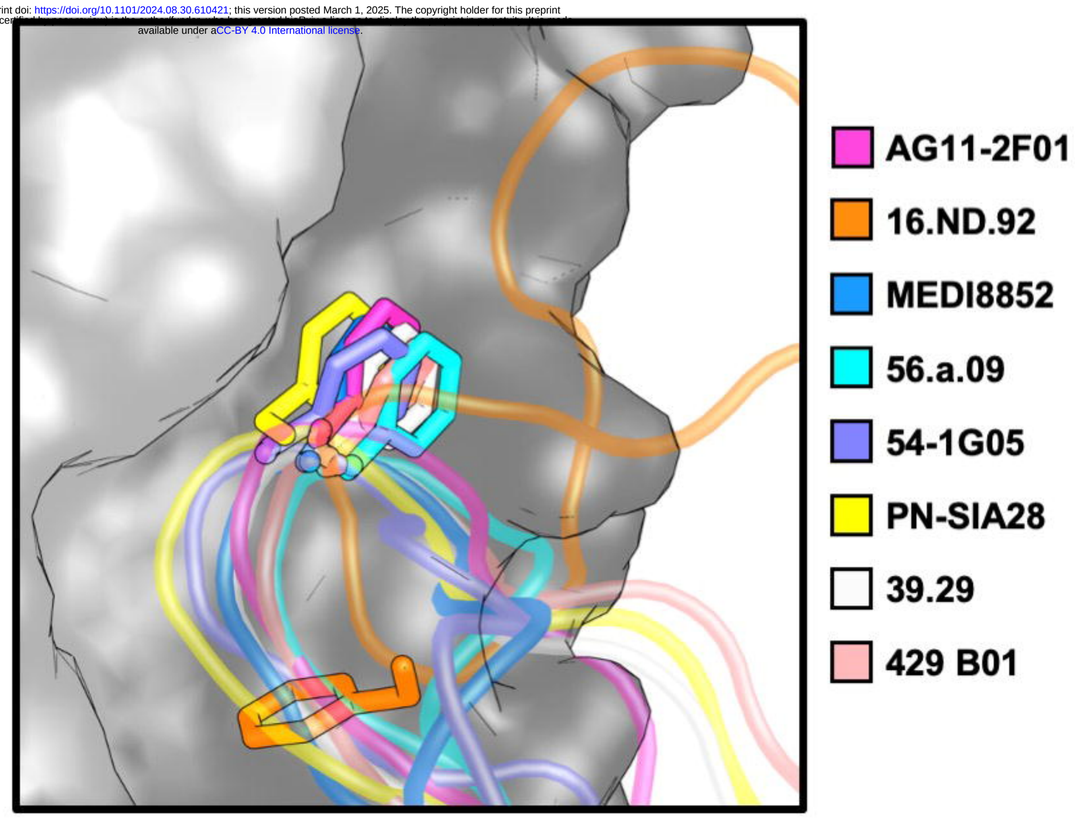

F

Paratope buried surface area

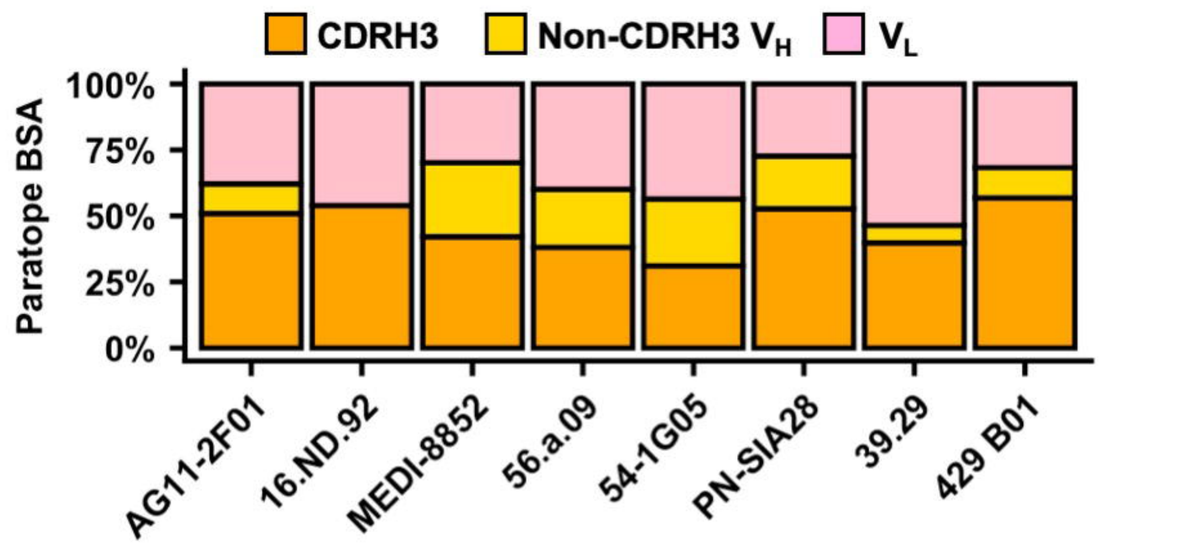

G

Contribution of IGHD3-3 to V_H paratope

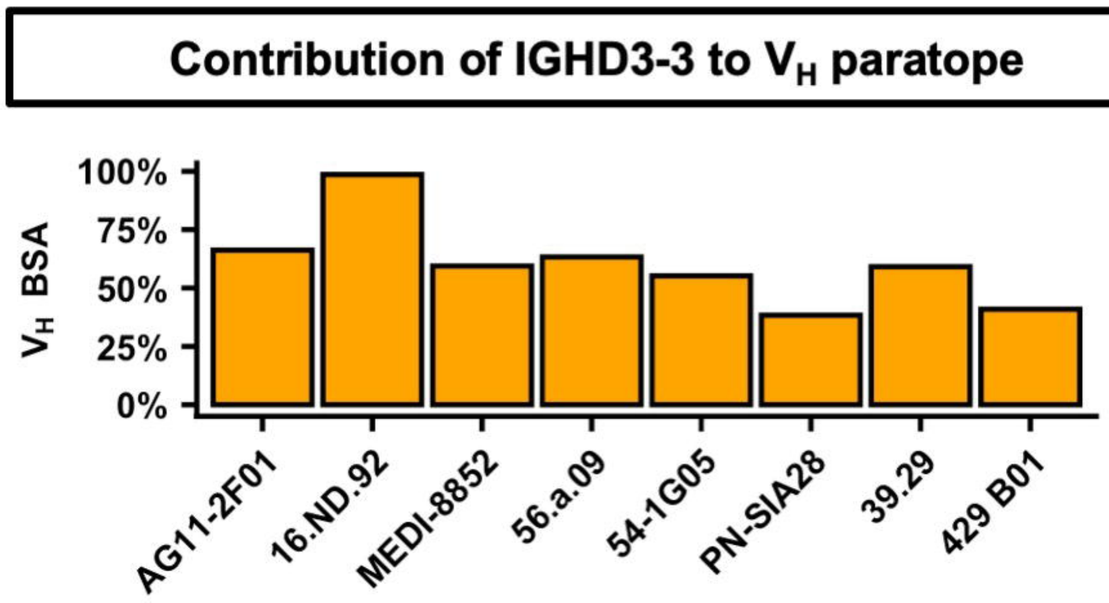

AG11-2F01 & 16.ND.92 *in vitro* activity

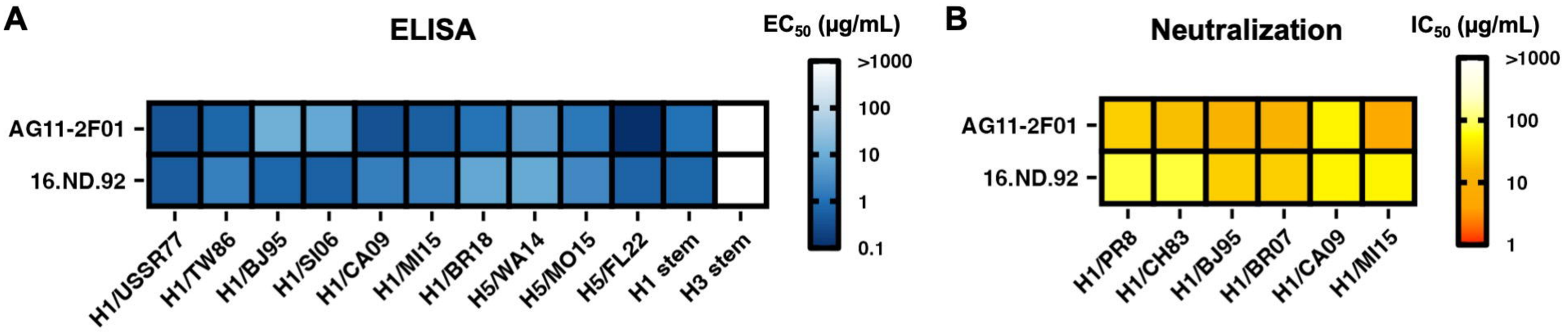

AG11-2F01 *in vivo* protection

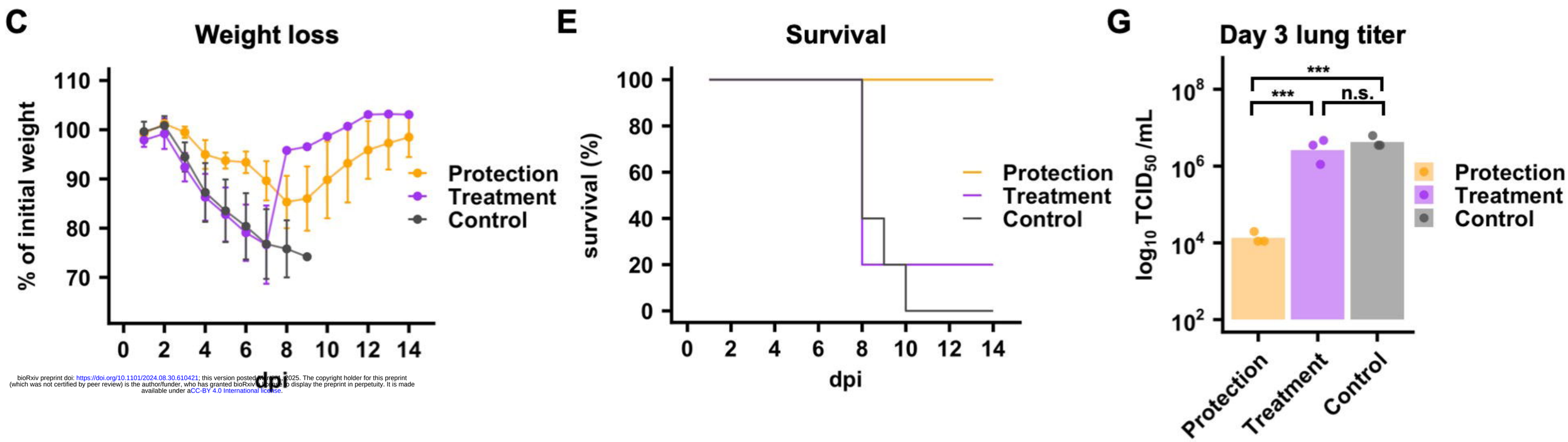

16.ND.92 *in vivo* protection